RESEARCH PAPER



Micro-mechanical analysis of sand-rubber mixtures with discrete element method

Pei Wang¹ · Junwei Gan¹ · Shuai Huang² · Bo Liu² · Changjie Xu¹

Received: 29 December 2024 / Accepted: 1 April 2025 / Published online: 10 June 2025 © The Author(s) 2025

Abstract

Incorporating sand with waste tire rubber as a new geotechnical material offers an effective solution to the global challenge of waste tire pollution. To investigate the complex mechanical behaviors of sand-rubber mixtures, DEM modeling of the sand-rubber mixtures, considering the realistic shape of particles and the deformability of rubber fibers is performed in this study. Microscopic parameters in the DEM are obtained through a comprehensive calibration process with results from the direct shear test, sliding test, and uniaxial tensile test. Next, a series of direct shear tests are simulated with sand-rubber mixtures of different rubber mass fractions and normal stresses, and the macroscopic behaviors, i.e., shear stress and volumetric strain of mixtures, are analyzed. At the microscale, the particle displacement fields, contact forces, internal forces of rubber fibers, and rubber fiber deformation are presented and investigated. In particular, a novel descriptor is proposed to assess the bending deformation of rubber fibers. The findings of this work enhance our comprehension of the mechanical behavior of sand-rubber mixtures and contribute to their application in engineering practices.

Keywords Discrete element modeling · Micro-macroscopic behavior · Particle shape · Sand-rubber mixtures

1 Introduction

The rapid growth of the automotive industry has led to an increasing accumulation of waste tires worldwide, which causes serious environmental issues. To address this problem, recycled tire rubber has been incorporated into construction materials for geotechnical and geological engineering applications, offering a sustainable solution to these environmental concerns. Waste tire rubber has been successfully used in roadbed and embankment filling [37, 52, 67, 76], railway foundations [29], and tunnel backfill [61, 62, 80]. Additionally, rubber waste has been

[8, 11, 65, 73] and backfill material for retaining walls [2, 20, 30, 44]. These applications demonstrate the significant potential of rubber mixtures in geotechnical engineering. Therefore, a comprehensive understanding of the mechanical behavior of sand-rubber mixtures is crucial for their application in engineering practices.

Experimental studies on sand-rubber mixtures have

employed as a rubber material in fiber-reinforced soil

highlighted the complexity of their mechanical behavior. For instance, Al-Rkaby [3] and Anbazhagan et al. [4] reported an increase in shear strength with added rubber content in triaxial tests. However, other studies noted a decrease in shear strength as rubber content increased in similar tests [40, 51]. Further research observed an initial rise in shear strength with rubber content, followed by a decline once a critical threshold was reached [1, 24]. These conflicting findings underscore the complexity of the mechanical properties in sand-rubber mixtures. Existing studies have provided insights into the mechanical evolution of sand-rubber mixtures. However, the distribution of deformation and internal force within rubber particles during shear processes has not been thoroughly explored. The macroscopic mechanical behavior of sand is often



Shuai Huang shuai.huang@polyu.edu.hk

[⊠] Bo Liu bo1liu@polyu.edu.hk

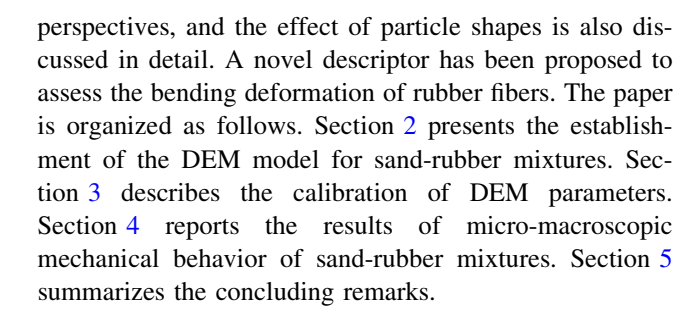
¹ Institute of Geotechnical Engineering, School of Civil Engineering and Architecture, East China Jiaotong University, Nanchang, Jiangxi, China

Department of Civil and Environmental Engineering, The Hong Kong Polytechnic University, Hung Hom, Kowloon, Hong Kong, China

closely tied to microscopic particle interactions, emphasizing the importance of microscopic analysis [39, 79]. In fact, the rubber fibers frequently undergo significant deformation, exerting a notable impact on the overall mechanical properties of the mixture [7, 23, 66]. Traditional experimental methods [25, 64] often struggle to explain the complex microscopic interactions and mechanical evolution of the sand-rubber mixtures. As a result, there is an urgent need for more advanced methods to accurately investigate both the macro- and micro-mechanical behaviors of sand-rubber mixtures, particularly to understand the force and deformation mechanisms of rubber within these systems.

The discrete element method (DEM) [21] has become a valuable tool for modeling granular materials [43, 47, 63], which has significantly advanced both macro- and micromechanical studies in the field [33-35, 69]. Recently, DEM has played a key role in understanding the behaviors of rubber materials [56] and sand-rubber mixtures [19, 27, 45]. To simplify the DEM model and improve computational efficiency, most of the current research employs spheres to simulate sand and rubber particles [28, 77]. While these studies offer some knowledge on the micro-mechanics of sand-rubber mixtures, the simplified sphere particle model fails to consider the influences of particle shape and the deformation of rubber particles. It is worth noting that some recent studies have attempted to model the irregular particle shapes of sand-rubber mixtures. Nevertheless, there are still some shortcomings, such as being limited to two dimensions [6] or adopting oversimplified particle shapes [18]. In addition, the effect of particle shape on the micro-macroscopic behavior of sandrubber mixtures has not been reported. Hence, it is necessary to develop a DEM model capable of precisely considering the realistic shapes of particles and the deformability of rubber fibers, aiming to enhance our understanding of the complex mechanical interactions in sand-rubber mixtures. The deformability feature of rubber fibers significantly influences the macroscopic behavior of sand-rubber mixtures [23]. The deformation modes of rubber fibers can be classified into axial deformation and bending. The axial deformation of rubber fibers has been effectively evaluated in [26]. However, a reliable descriptor for bending deformation is still missing, which makes it challenging to comprehensively evaluate deformation feature of rubber fibers.

This work presents a DEM modeling approach of the sand-rubber mixtures in consideration of the realistic shape of particles and the deformation of rubber fibers. The DEM parameters of the sand-rubber mixtures are carefully calibrated by a series of laboratory tests at the single particle scale. The shear behavior of sand-rubber mixtures is analyzed from both macroscopic and microscopic



2 DEM model of sand-rubber mixtures

2.1 Acquisition of sand-rubber mixture morphology

In this work, Fujian standard sand is chosen for subsequent experiments and DEM simulations due to its uniform gradation and excellent engineering properties [10, 12, 31]. As shown in Fig. 1a, sand particles with sizes ranging from 0.9 mm to 2.1 mm are obtained by sieving. To acquire particle morphology, about 200 sand particles filled in a cylindrical container which is subjected to X-ray CT scan [14, 16, 32, 33, 42]. Then, image processing is then performed to segregate individual particles in the image and reconstruct their shapes. Then, image processing is then performed to segregate individual particles in the image and reconstruct their shapes which will serve as shape templates in DEM modeling. It should be noted that approximately 200 sand particle shapes are used in the DEM simulations. For the sake of brevity, the image processing procedures will not be discussed in this work, whereas interested readers are referred to this reference for details [34]. Figure 1b illustrates a number of sand particles represented by surface triangle mesh.

The rubber fibers are derived from recycled waste tires, processed by cutting shredded tire materials. As shown in Fig. 2, rubber particles with the elongated shape are selected for investigation in this work. The rubber fibers are featured the same size of 1.0 mm in height and width and 4.0 mm in length.

2.2 Particle models

Particle shapes and inherent mechanical properties can significantly impact the mechanical behavior of the bulk granular materials. In this study, sand-rubber mixtures are composed of irregularly shaped Fujian sand and elongated and deformable rubber fibers. This complex composition requires careful selection of particle models in the DEM simulations. For sand particles, the clump method, in which particles are modeled by a rigid assembly of spheres, is utilized to approximate the real shape of sand. The most



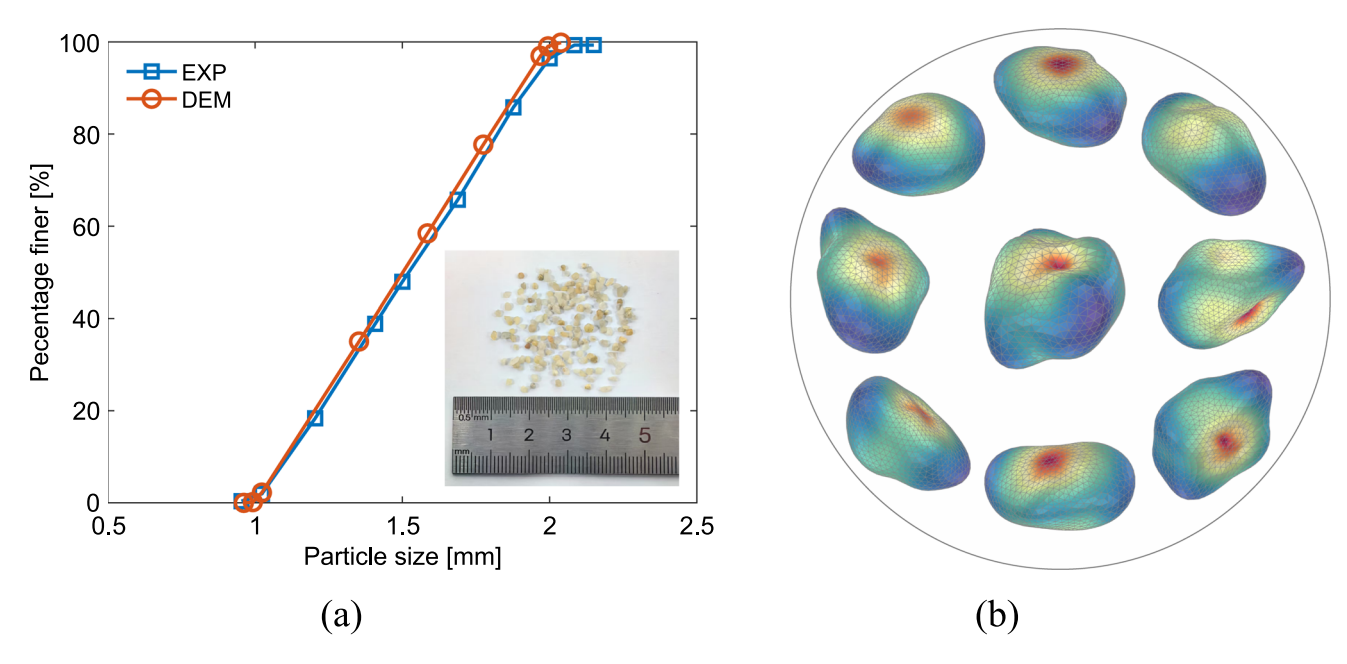


Fig. 1 Sand characteristics: a particle size distribution and b particle shapes

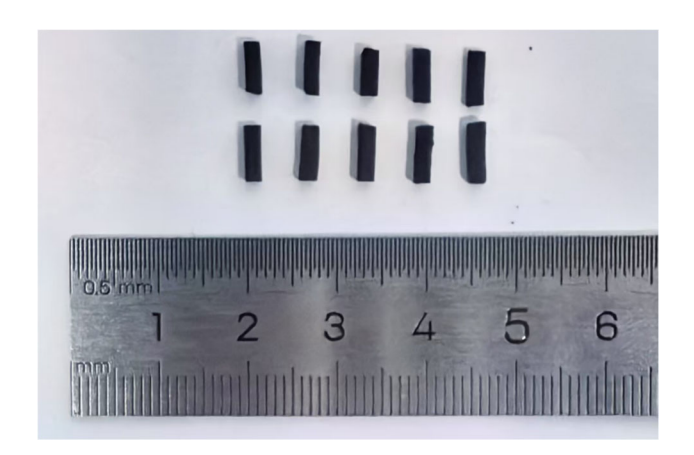


Fig. 2 Rubber fibers used in experiments and DEM simulations

notable advantages of this particle model are its computational efficiency and straightforward contact detection algorithms. Specifically, the realistic shape templates of sand particles are reconstructed by the bubble packing approach. The approximation accuracy in this approach can be adjusted by two key parameters: distance and ratio. The distance influences the smoothness and angularity of particle surfaces, while the ratio defines the size ratio between the smallest and largest spheres. Figure 3 illustrates the effects of these two parameters on the shape of a particle template. To achieve a balance between shape approximation accuracy and computational efficiency, the ratio and distance are set respectively as 0.55 and 140, leading to a total of 25 spheres in the particle.

Regarding the rubber fibers, the cluster method is utilized to describe the highly deformable feature of rubber

particles [15, 17, 71, 75]. A cluster is formed by bonding two or more spheres together, allowing axial, shear, twisting, and bending behavior at the bonds. Thus, the rubber particles can be accurately represented in the simulations. Figure 4 shows the cluster of a rubber fiber, composed of seven overlapping spheres to approximate the elongated particle shape. It is important to note that both the size and number of pebbles influence the rubber calibration parameters. While increasing the number of pebbles in simulations can provide a more accurate representation of the rubber shape, it may also result in a substantial rise in computational costs.

2.3 Contact models

In DEM, the interaction between particles is governed by contact models. As illustrated in Fig. 5, four types of contacts are considered in the DEM model for sand-rubber mixture, i.e., the sand-sand contact (S–S), sand-rubber contact (S–R), rubber-rubber contact (R–R), and bonds within the rubber clusters (intra-particle contacts). The S–S, S–R, and R–R contacts are governed by the linear elastic model and are given as follows:

$$k_n = AE^*/L \tag{1}$$

$$k_s = k_n / \kappa^* \tag{2}$$

$$F_n = k_n \delta_n \tag{3}$$

$$F_t = \min(F_t^0 + k_t \Delta \delta_t, \mu F_n) \tag{4}$$

$$M_c = 0 (5)$$



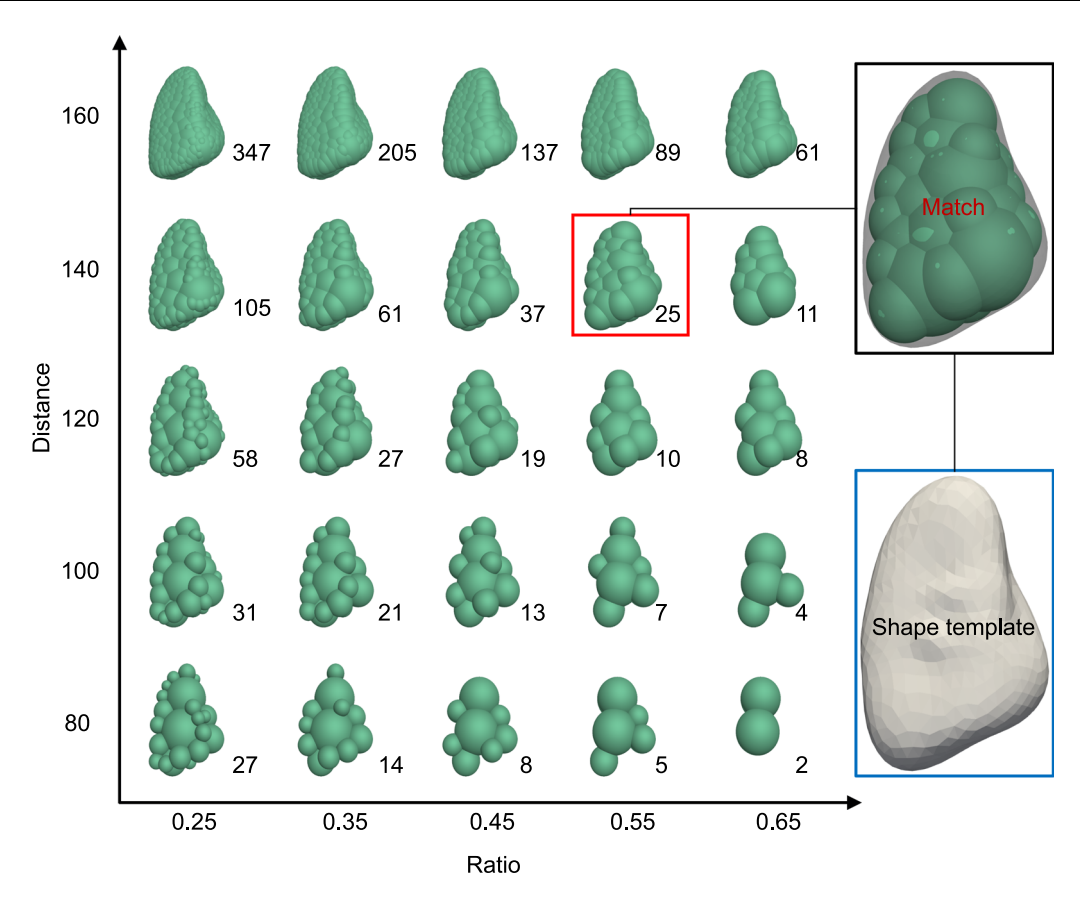


Fig. 3 Effects of ratio and distance on particle shape approximation

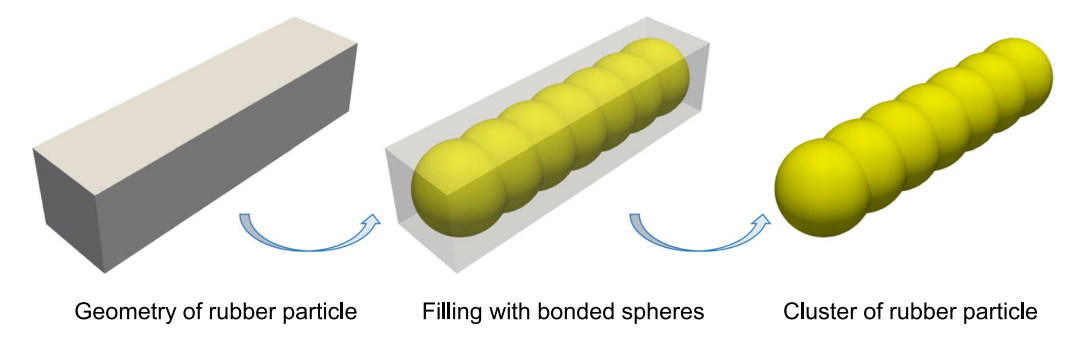


Fig. 4 Illustration of cluster method for rubber fibers

where E^* is the effective modulus, L represents the distance between the centers of the two contacting spheres, and A denotes the cross-sectional area of the smaller sphere between them. κ^* is the ratio of normal to tangential stiffness, while F_n and F_t are the normal and tangential forces, respectively; k_n and k_t are the normal and tangential stiffness, respectively; μ is the friction coefficient; F_t^0 represents the tangential force at the beginning of the current DEM cycle, and M_c is the moment.

The linear parallel-bond model is adopted for the contacts within the rubber. The force and moment in the parallel bond are updated as

$$F_n = F_{n0} + \overline{k_n} A' \Delta \delta_n \tag{6}$$

$$F_t = F_{t0} + \overline{k_t} A' \Delta \delta_t \tag{7}$$

$$M_b = M_{b0} - \overline{k_n} I \Delta \theta_b \tag{8}$$

where F_n , F_t , and M_b are the normal force, tangential force, and moment of the bond, respectively; the subscript θ indicates the force or moment obtained from the previous cycle; A' is the cross-sectional area moment of inertia; I is the moment of inertia of the parallel bond cross section; while $\Delta \delta_n$, $\Delta \delta_s$, and $\Delta \theta_n$ correspond to the increments in the normal displacement, shear displacement, and bending displacement, respectively.



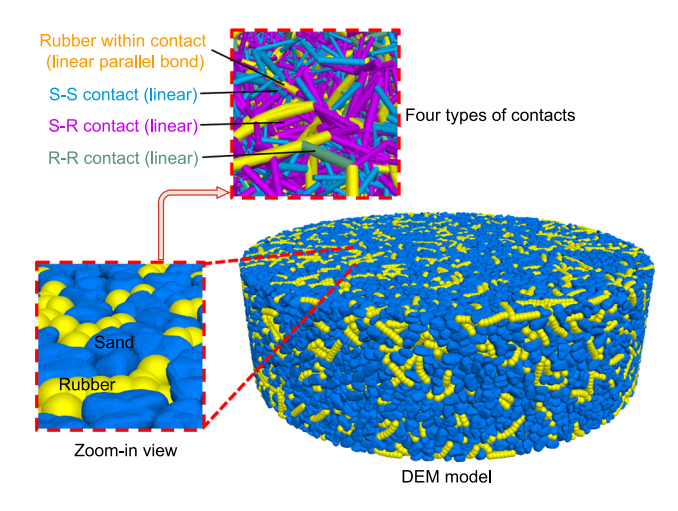


Fig. 5 Four contact types in the DEM model for sand-rubber mixture

2.4 DEM specimen preparation

In the direct shear test, sand particles and rubber particles are mixed and filled into a cylindrical container with a diameter of 70 mm and a height of 20 mm. To ensure adequate mixing of sand and rubber, the specimen is divided into four layers and then compacted using the multi-layer compaction method [38]. In each layer, sand particles and rubber particles are randomly generated. The porosity of mixtures is controlled by moving the top plate to reach the specified heights (e.g., 5, 10, 15, and 20 mm). It should be noted that the gravity and inter-particle friction coefficients are assigned to the model once the particle sample has finished assembling. This contributes to removing potential cavity and improving sample homogeneity. Upon completion of sample generation, the normal stress is applied to the specified values (e.g., 50, 100, and 150 kPa) using servo control and is maintained during the shear process (Fig. 6).

To evaluate the effect of the mass fraction of rubber fibers, samples with the mass fractions of 0%, 10%, 20%, 30% and 40% are prepared. The rubber mass fraction is defined as the ratio of the mass of rubber fibers to the mass of the mixture. Figure 7 illustrates the DEM specimens for sand-rubber mixture with different rubber mass fractions,

in which sand and rubber particles are well mixed with rubber fibers evenly distributed within the specimen.

3 Parameter calibration and model validation

3.1 Calibration produce

The accuracy of DEM simulations highly relates to the reasonableness of model parameters. Therefore, the input DEM parameters are calibrated through a series of laboratory tests, following a calibration procedure similar in [77, 78]. As shown in Fig. 8, the model parameters are divided into three groups: known, measured, and calculated parameters. Within the group of known parameters, the Poisson's ratios of sand and rubber are 0.2 and 0.48, respectively. The damping coefficient, which minimally affects simulation outcomes under quasi-static conditions, is set to 0.7, as recommended by [26]. Within the group of measured parameters, the densities of sand and rubber particles are recorded at approximately 2650 and 1700 kg/ m³, respectively. The effective modulus and friction coefficients of the sand-rubber mixtures are determined through a series of laboratory tests, including direct shear tests, tensile tests, column collapse tests, and sliding tests, which will be elaborated later. The calculated parameters can be derived by substituting the known and measured parameters into the equations presented in Fig. 8. Interested readers are referred to [41] for more details about the calculation schemes.

3.2 Effective modulus

To calibrate the effective modulus of sand-sand contacts (E_s) , the direct shear test is conducted on pure sand utilizing an automatic direct shear apparatus, as shown in Fig. 9. The specimen in the direct shear test has a cylindrical shape with a diameter of 70 mm and a height of 20 mm. The sample size used in the DEM model is consistent with that of the laboratory tests. Additionally, both the tests and simulations conducted in this study meet the size

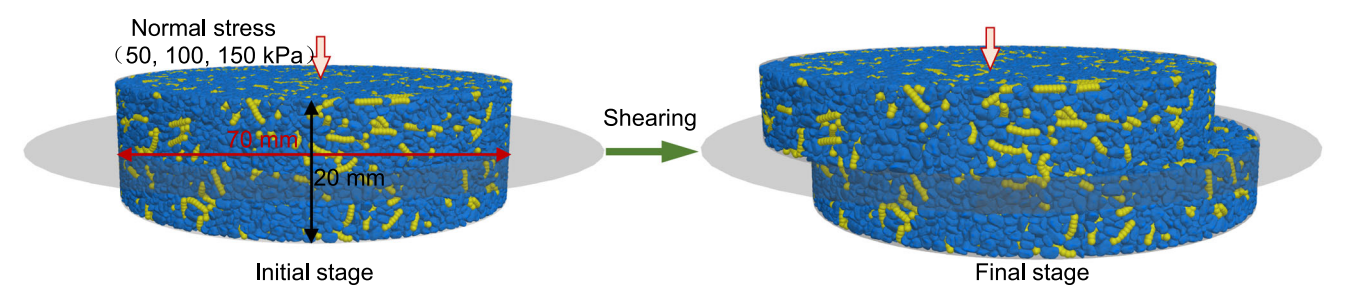


Fig. 6 Discrete element model of a direct shear test specimen



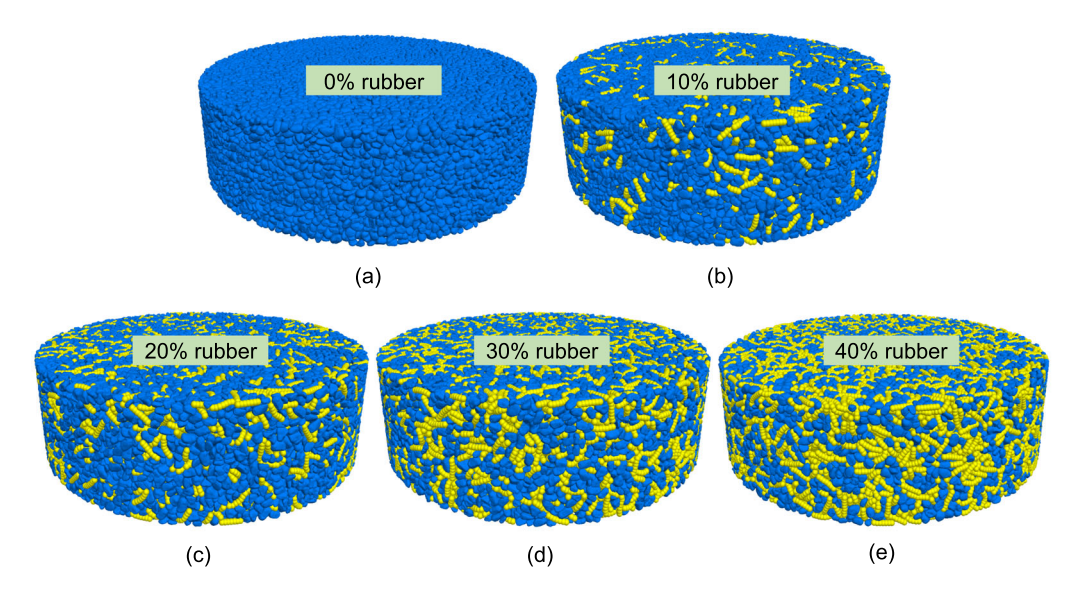


Fig.7 DEM specimens of sand-rubber mixtures with different rubber content: a 0% rubber content, b 10% rubber content, c 20% rubber content, d 30% rubber content, e 40% rubber content

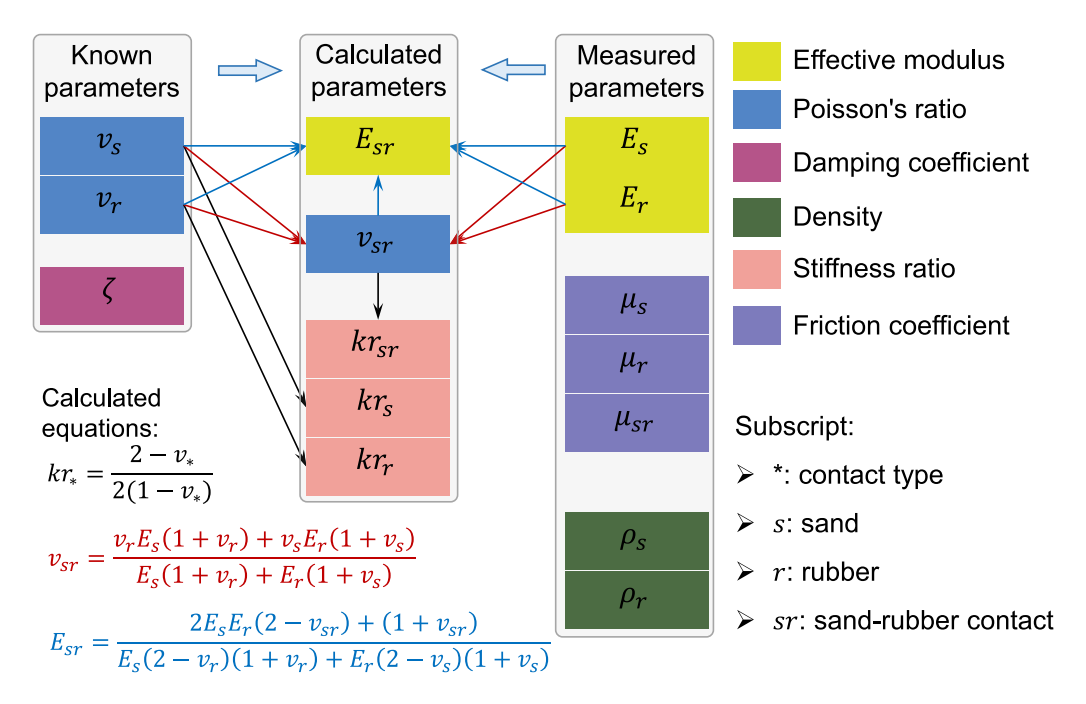


Fig. 8 Calibration procedure of input parameters for the DEM model

requirements outlined in ASTM D3080/D3080M-11 [22]. During preparation, the specimen is slightly compacted using a pestle to eliminate potential voids and enhance sample uniformity. Subsequently, the specimen is consolidated under designated confining pressures. Three normal stresses are used, i.e., 50, 100 and 150 kPa, and the porosity of the model is 0.19. Then, the specimen is sheared at a rate of 0.8 mm/min by applying a lateral velocity to the lower part of the shearing cell.

Figure 10 depicts the evolution of the shear stress during shearing at different normal stresses. Herein, the shear

strain is the ratio of the lateral displacement of the lower part of the shear cell to the specimen diameter. The shear stress gradually increases as the shear strain approaches approximately 5%, after which it becomes stable and exhibits an almost constant value [48]. The shear behavior derived from the DEM simulations show a good match with the results obtained from the laboratory tests. The calibrated effective modulus of the sand-sand contacts is 300 MPa.

To calibrate the effective modulus of rubber-rubber contacts, we conducted uniaxial tensile tests on rubber



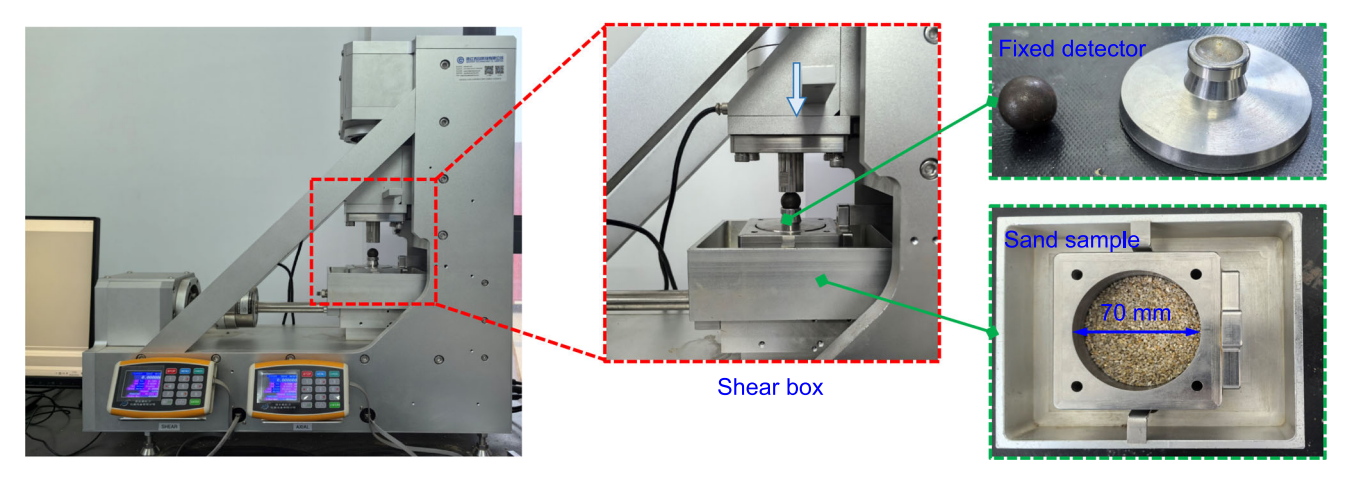


Fig. 9 Apparatus and specimens for the direct shear test

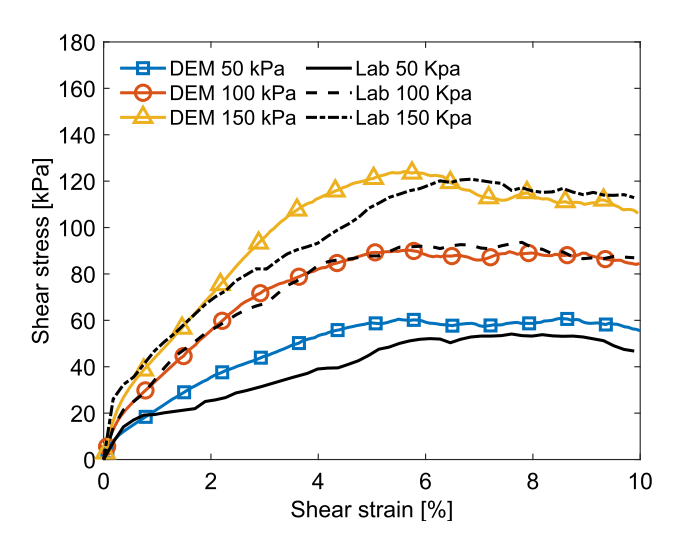


Fig. 10 Comparison of shear stress and shear strain relationships between laboratory tests and DEM simulations at three different normal stresses

samples using a single axis tensile tester. Figure 11 illustrates the setup of the uniaxial tensile test and the corresponding model of the rubber fiber in DEM, where the sizes of the rubber fiber in the tests and simulations are both 4 mm. During the tensile test and DEM simulation, the bottom of the rubber remained fixed, while a constant upward velocity was applied at the top, gradually stretching the rubber until reaching the target strain. The calibrated normal and shear stiffness of the parallel bond are 9×10^8 N/m³ and 9×10^8 N/m³, respectively [26]. The calibrated effective modulus of the rubber–rubber contacts is 1.1 MPa. As illustrated in Fig. 11, the force–displacement relationships between the DEM simulations and the laboratory tests are in good agreement.

3.3 Friction coefficients

In the sand-rubber mixtures, three friction coefficients are considered, i.e., sand-sand contacts (μ_s) , rubber-rubber contacts (μ_r) , and sand-rubber contacts (μ_{sr}) . The friction coefficient of sand-sand can be determined by direct shear tests and the friction angle is calculated to be approximately 28.81° and verified by column collapse tests [49], as shown in Fig. 12. The measured angle of repose is about 29°, which corresponds to a friction coefficient of about 0.55.

The friction coefficients of rubber-rubber contacts (μ_r) and sand-rubber contacts (μ_{sr}) are determined by the sliding tests. As shown in Fig. 13, a flat rubber block is affixed to a slope, and a sand/rubber particle is placed on the surface of rubber block. The inclination of the slope is gradually increased, and the angle at which the sand/rubber particle starts to slip off is recorded. A similar numerical model of the sliding test is generated in DEM, in which the inclination angle is the same as the recorded value in the test. The initial friction coefficient between the particle and the bottom is set as large as 1.0 in the model. Next, the coefficient is gradually decreased until the particle movement initiates. The lowest coefficient that maintaining the particle static is determined as the friction coefficient between the particle and the surface. Notably, approximately 200 sand particles with diverse shapes undergo the sliding test, and the average friction angle is adopted in the DEM simulation. The friction coefficients for rubber-rubber and sand-rubber contacts obtained through the above method are 0.71 and 0.52, respectively.

After the measured parameters are determined by a series of laboratory tests, the calculated parameters are calculated using the equations in Fig. 8, it is important to note that no breakages of the rubber fibers are observed after completing the test. As a result, the tensile strength and cohesion are set to very high values to remove the



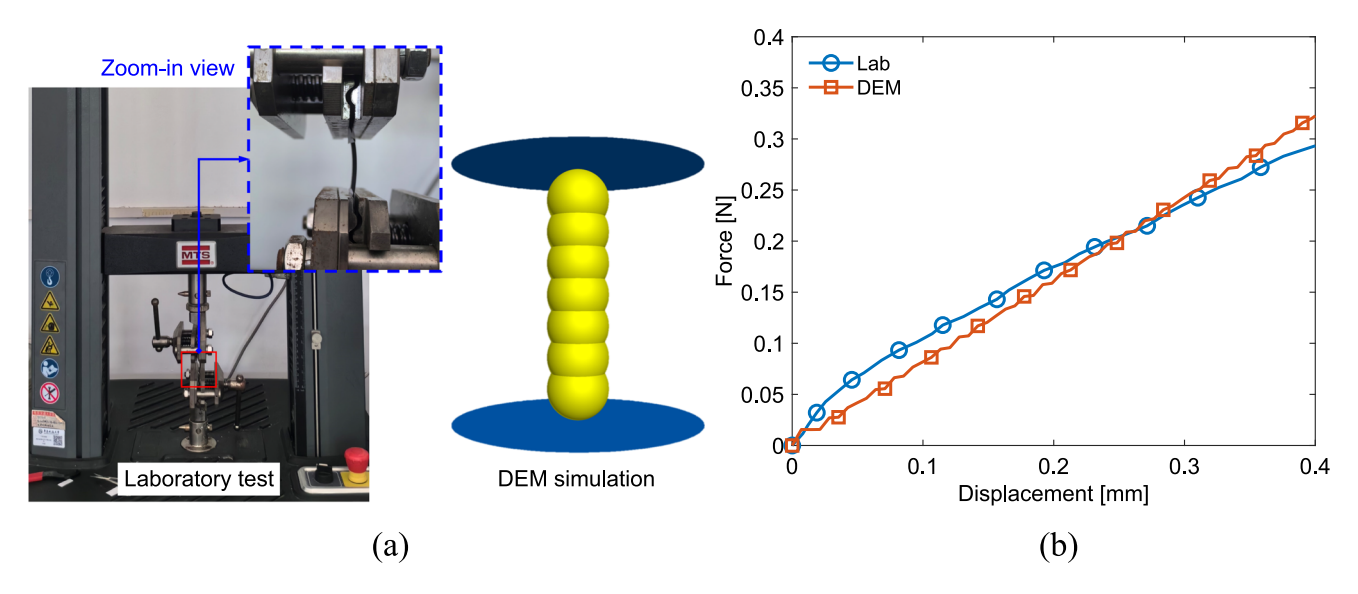


Fig. 11 Laboratory test and DEM simulation for the uniaxial tensile test of the rubber fiber: a model setup, b force-displacement relationships



Fig. 12 Column collapse test of sand

breakage within the rubber fiber [15, 18]. All the DEM model parameters of sand-rubber mixtures are listed Table 1.

3.4 Experimental validation

To validate the effectiveness of the DEM model, a direct shear test is performed on sand-rubber mixtures. The rubber mass fraction in the specimen is 10%, with a normal stress of 100 kPa and a porosity of 0.19. A DEM model with the same dimension, particle size, rubber mass and normal stress is established for comparison. Figure 14 illustrates the stress–strain curves from the laboratory test and DEM simulation. It is evident that the shear stress initially increases, reaching a peak value at shear strain of

approximately 8%, followed by a gradual decrease. The comparison between the experimental and simulated results demonstrates a good agreement, confirming that the DEM model and the associated parameters can effectively reflect the mechanical behavior of sand-rubber mixtures.

4 Simulation results and discussions

This section presents the results of DEM simulations of direct shear tests on sand-rubber mixtures with various rubber mass fractions and normal stresses, including both macroscopic and microscopic mechanical behaviors. Additionally, the effect of the particle shape on shear behavior with the mixtures is discussed.

4.1 Macroscopic analysis

The effects of varying normal stresses and rubber mass fractions on shear behaviors are depicted in Fig. 15. During the shearing, pure sand samples first exhibit a strain hardening behavior and then strain softening after peak shear stress, consistent with findings in references [53, 5755]. As

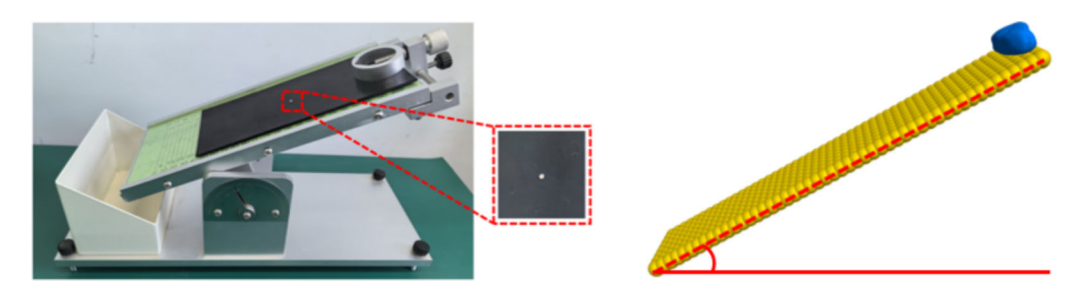


Fig. 13 Sliding tests for the friction coefficients of sand-rubber and rubber-rubber contacts



Table 1 DEM model parameters of sand-rubber mixtures

Parameter	Value
Effective modulus of sand-sand contacts, E_s (MPa)	300
Stiffness ratio of sand-sand contacts, kr_s	1.125
Friction coefficient of sand-sand contacts, μ_s	0.55
Effective modulus of rubber–rubber contacts, E_r (MPa)	1.1
Stiffness ratio of rubber–rubber contacts, kr_r	1.461
Friction coefficient of rubber–rubber contacts, μ_r	0.71
Effective modulus of sand-rubber contacts, E_{sr} (MPa)	2.19
Stiffness ratio of sand-rubber contacts, kr_{sr}	1.46
Friction coefficient of sand-rubber contacts, μ_{sr}	0.52
Parallel bond normal stiffness of a rubber particle, $\overline{k_n}$ (N/m ³)	9 × 10 ⁸
Parallel bond shear stiffness of a rubber particle, $\overline{k_s}$ (N/m ³)	9 × 10 ⁸
Density of sand particles, ρ_s (g/cm ³)	2.65
Density of rubber particles, ρ_r (g/cm ³)	1.7
Global damping ratio, ξ	0.7
Tensile strength of rubber (MPa)	1×10^{194}
Cohesion of rubber (MPa)	1×10^{194}

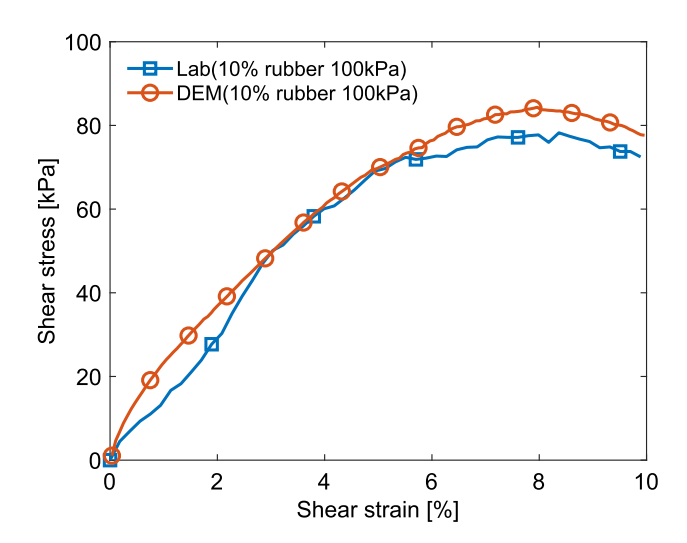


Fig. 14 The comparison of the stress-strain curves in the direct shear test between laboratory test and DEM simulation

the rubber mass fraction increases, the trend of strain softening in the sand-rubber mixtures gradually weakens and eventually disappears when the rubber mass fraction exceeds 30%. The continuous strain hardening trend becomes more pronounced, especially under higher normal stresses. Additionally, greater rubber content results in a marked reduction in the stiffness of the specimens, and therefore a large shear displacement is needed to reach the peak shear stress. The above findings align with [5, 18, 23]. For the volumetric deformation, the specimen exhibits a

significant dilative behavior at the normal stress of 50 kPa, as shown in Fig. 15b. However, with the normal stress increases to 100 kPa and 150 kPa, the dilation is suppressed. This phenomenon is more noticeable when the rubber mass fraction is high. For instance, the specimen with a rubber mass fraction of 40% and a normal stress of 150 kPa exhibits contraction during almost the entire direct shearing process. In fact, due to the lower modulus of elasticity of rubber–rubber and sand-rubber contacts, specimens with higher rubber mass fractions exhibit greater compressibility. The addition of rubber fibers in the specimen facilitates the filling of voids between sand particles, making the material more prone to deformation during shear.

4.2 Microscopic analysis

4.2.1 Particle displacement

Figure 15 indicates that the volumetric change of the sandrubber mixtures is correlated with both the rubber mass fraction and the normal stress. In this section, the displacement of particles is extracted to gain more insights into this relationship from a microscopic perspective. Figure 16 illustrates the particle vertical displacement field of sand-rubber mixtures with different rubber mass fractions at the end of the direct shear test. The negative values indicate downward vertical displacement, vice versa. Figure 16 shows that the particles with greater vertical displacement mainly concentrate in the upper part of the shear box, and the downward displacement becomes increasingly prominent with higher rubber mass fractions. Figure 17 shows the particle vertical displacement of sand-rubber mixtures under different normal stresses at the end of the direct shear test. As the normal stress increases, the overall trend of downward displacement becomes more pronounced, aligning with macroscopic observations of decreased volumetric dilation.

4.2.2 Contact types and orientations

The inter-particle contacts in the DEM model are classified into strong and weak contacts [36, 46, 59]. Herein, contacts are differentiated by the mean of contact forces: those exceeding the mean value are classified as strong contacts, whereas those falling below the it are labeled as weak ones [18, 50, 54, 58]. Figure 18 illustrates distribution of different contact types in strong contact networks of the specimens at the end of the direct shear test. In specimens with low rubber mass fractions (i.e., 10%), strong contacts are predominantly composed of S–S contacts, with a much lower fraction of S-R contacts and nearly absent R-R contacts. With an increase in the rubber mass fraction, the



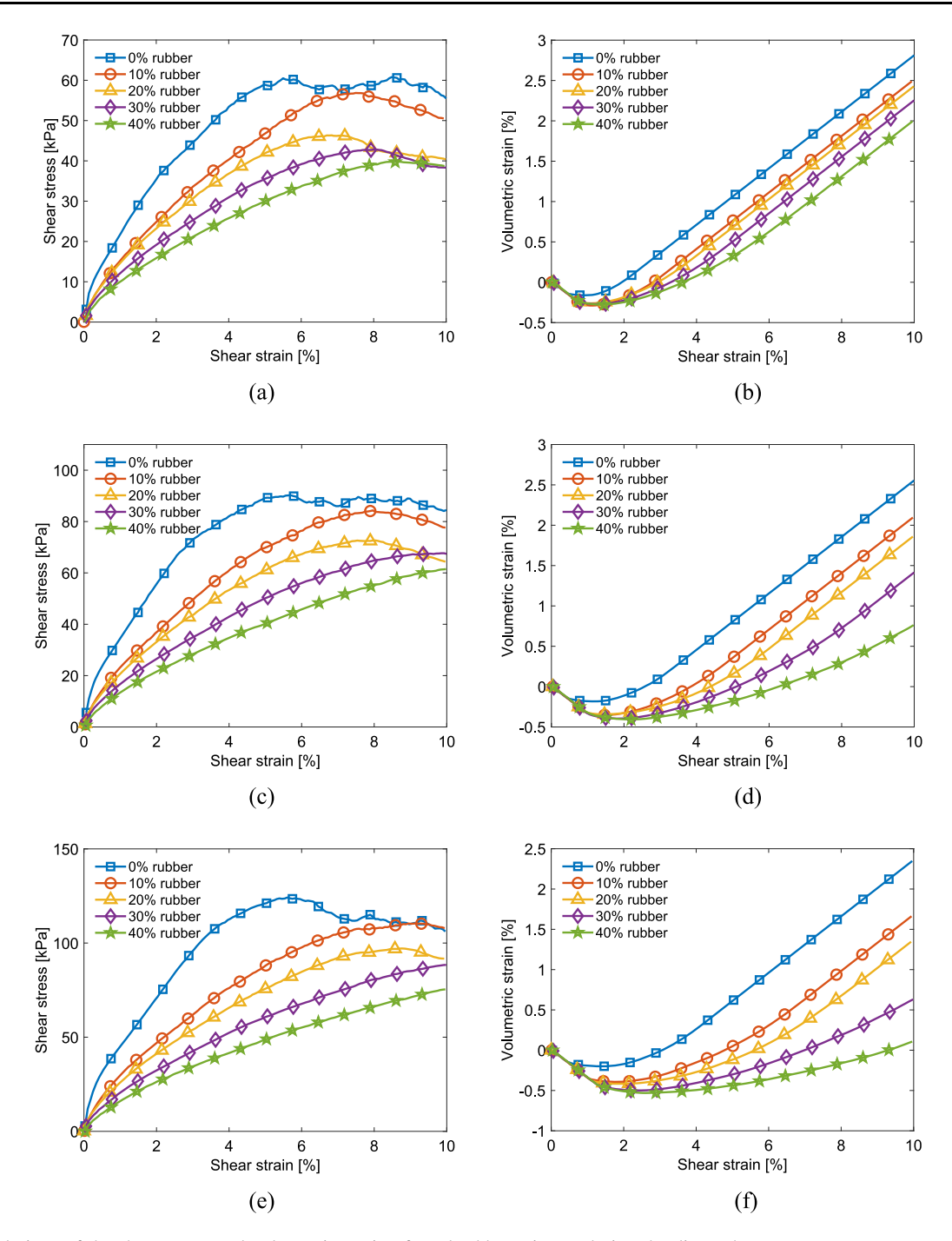


Fig. 15 Evolutions of the shear stress and volumetric strain of sand-rubber mixture during the direct shear test

proportion of S–S contacts decreases within the strong contact network, while the proportions of S-R and R-R contacts increase. When the rubber mass fraction reaches 40%, the S-R contact becomes the dominant component in the strong contact network. This phenomenon signifies the major role of rubber in resisting shear force, synergistically governing the properties of the mixture with other contact types. The impact of normal stress is comparatively minor, as demonstrated by similar relative proportions among

three different contact types under different normal stresses.

Furthermore, the distribution of contact normal orientation of the sand-rubber mixtures is visualized in Fig. 19. The distribution presents a dominant alignment in the vertical direction in the initial stage, transitioning to an inclined angle with the horizontal direction at the end. This phenomenon is attributed to the shear stress induced by shearing. In addition, the anisotropy in contact normal



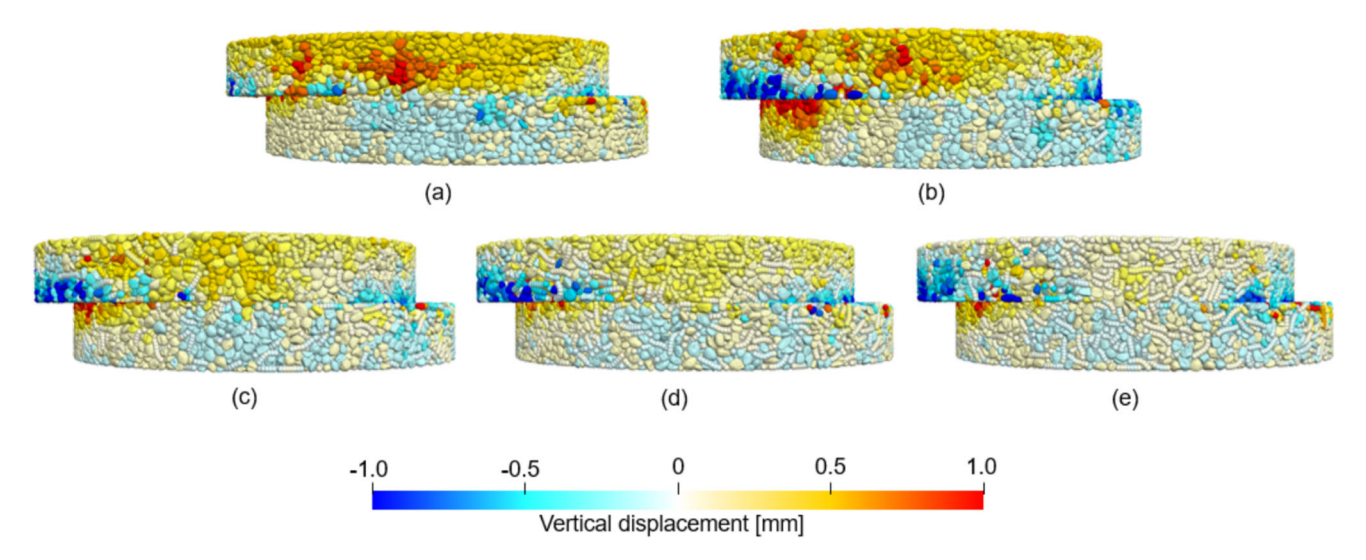


Fig. 16 Vertical displacement of particles in samples with different rubber mass fractions under 100 kPa normal stress: **a** pure sand, **b** 10% rubber, **c** 20% rubber, **d** 30% rubber, and **e** 40% rubber

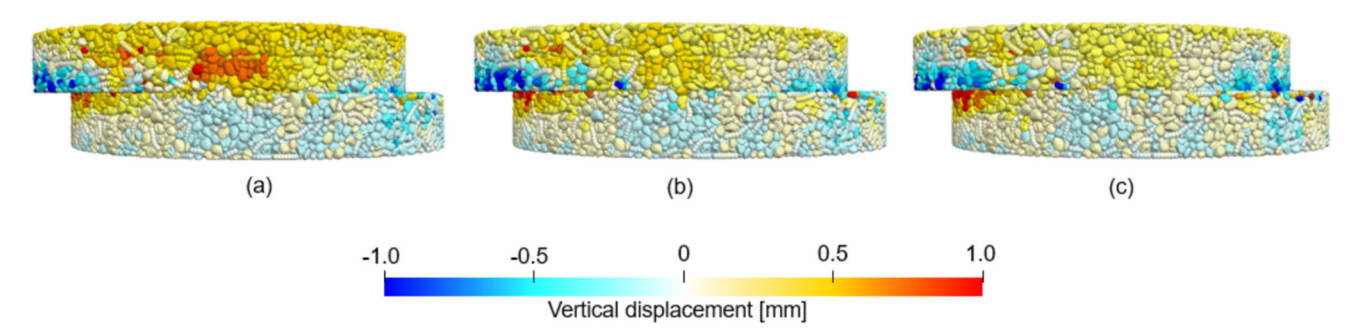


Fig. 17 Vertical displacement of particles in samples with a rubber mass fraction of 20% under the normal stress of **a** 50 kPa, **b** 100 kPa, and **c** 150 kPa

orientation increases when the normal stress or the rubber mass fraction is increased.

4.2.3 Analysis of internal force of rubber fiber

In addition to the inter-particle contacts (i.e., S–S, S-R, and R-R), the intra-particle contacts (i.e., the contacts between contacting spheres within a rubber fiber) are extracted for further analysis of the mechanical behavior of rubber fibers during the shearing process. In this work, two indicators, namely the normalized average tensile force (A_T) and the ratio of the tensile to the compressive force (R_{TC}) , proposed by Yang et al. in [74], are utilized to describe the internal forces within rubber fibers. A_T reflects the development of tensile forces within the rubber, while R_{TC} describes the main type of force inside the rubber. As depicted in Fig. 20a, the average tensile force decreases with the increase of rubber mass fraction under the same normal stress. This indicates that the tensile force experienced by the rubber is primarily induced by the surrounding sand particles. Additionally, the tensile force is positively

correlated with the normal stress. This may be due to the fact that the higher normal stress increases the compressive and shear forces at the sand-rubber contacts and thus stretches rubber fibers, leading to stronger tensile force within the fibers. Figure 20b illustrates the R_{TC} of rubber fibers at the end of shearing. The results show that the rubber fibers exhibit a tensile state in specimens when the rubber mass fraction and normal stress are low. As the rubber mass fraction and normal stress increase, the internal force of the rubber fibers gradually transforms from tension to compression. When the rubber mass fraction surpasses 30%, the influence of normal stress on the compressive force within the rubber fibers is notable, yet it has minimal impact on the tensile force. In light of the deformable properties of the rubber fiber, it can be inferred that higher normal stress leads to greater compression of the rubber, resulting in a reduction in the overall stiffness of the sample and more pronounced volumetric compression.



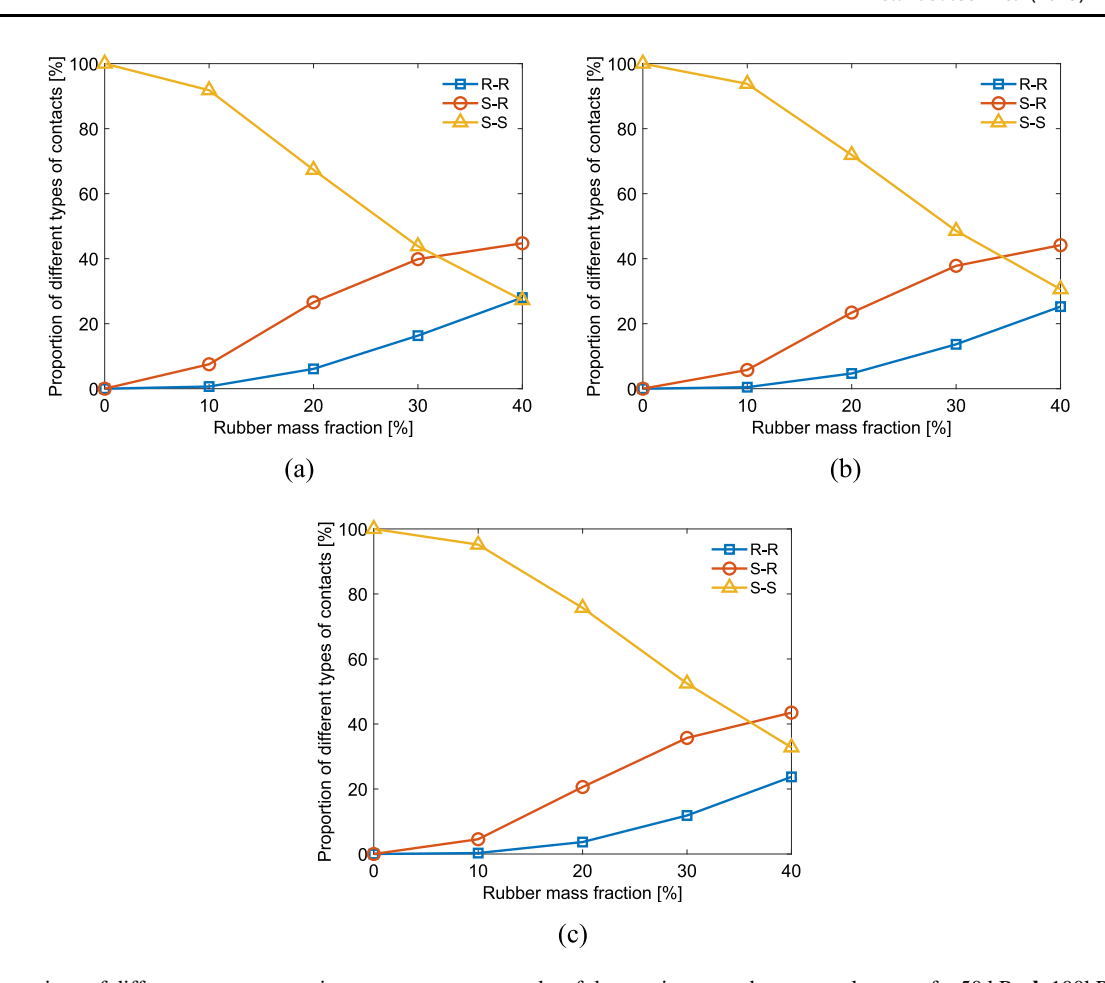


Fig. 18 Proportions of different contact types in strong contact networks of the specimens under a normal stress of a 50 kPa, b 100kPa, and c 150 kPa at the end of the direct shear test

4.2.4 Evaluation of rubber fiber deformation

In view of the deformability of rubber and its influence on the unique mechanical behavior of sand-rubber mixtures, a comprehensive understanding of rubber deformation during direct shear is crucial for interpreting the micro-mechanical properties of the mixture. As shown in Fig. 21a and b, the deformation modes of rubber fibers can be classified into two types: axial deformation and bending, while Fig. 21c presents the realistic deformation morphology diagrams of rubber fibers extracted from the DEM simulation. The former can be evaluated by comparing the current length (I) of the fiber and its initial length (I_0) [26]. Specifically, a rubber fiber is compressed when I/I_0 is less than 1.0 and stretched when I/I_0 is greater than 1.0. However, a robust descriptor to evaluate the bending of rubber fibers is missing in existing studies. Therefore, a novel descriptor, the average bending angle, is proposed to assess the bending of the rubber fibers. The definition of the average bending angle is illustrated in Fig. 22. For the first three neighboring spheres within the rubber fiber, the spherical centers form a local bending angle (α_1) .

Similarly, the local bending angle, α_i , can be derived for any three neigoubhouring particles, resulting a total number of n-2 local bending angles by traversing all neighbouring spheres, where n is the number of spheres in this rubber fiber. Note that the local bending angle ranges from 0° to 180° . Finally, the bending angle $(\overline{\alpha})$ of the rubber fiber is calculated as the average of all local bending angles of this rubber fiber. According to the definition, a bending angle close to 180° implies that the rubber fiber undergoes very limited bending.

Figure 23 shows the evolution of the average length ratio of all of the rubber fibers within the specimens under different normal stresses. The results indicate that, for a given specimen, the length change of rubber fibers is very slight during the test. The rubber mass fraction plays a more significant role in determining the average length ratio. An increase in the rubber mass fraction decreases the tensile deformation of rubber induced by shearing. For instance, the rubber fibers of the specimen with a rubber mass fraction of 40% and a normal stress of 150 kPa consistently exhibit a compression deformation during the direct shearing process.



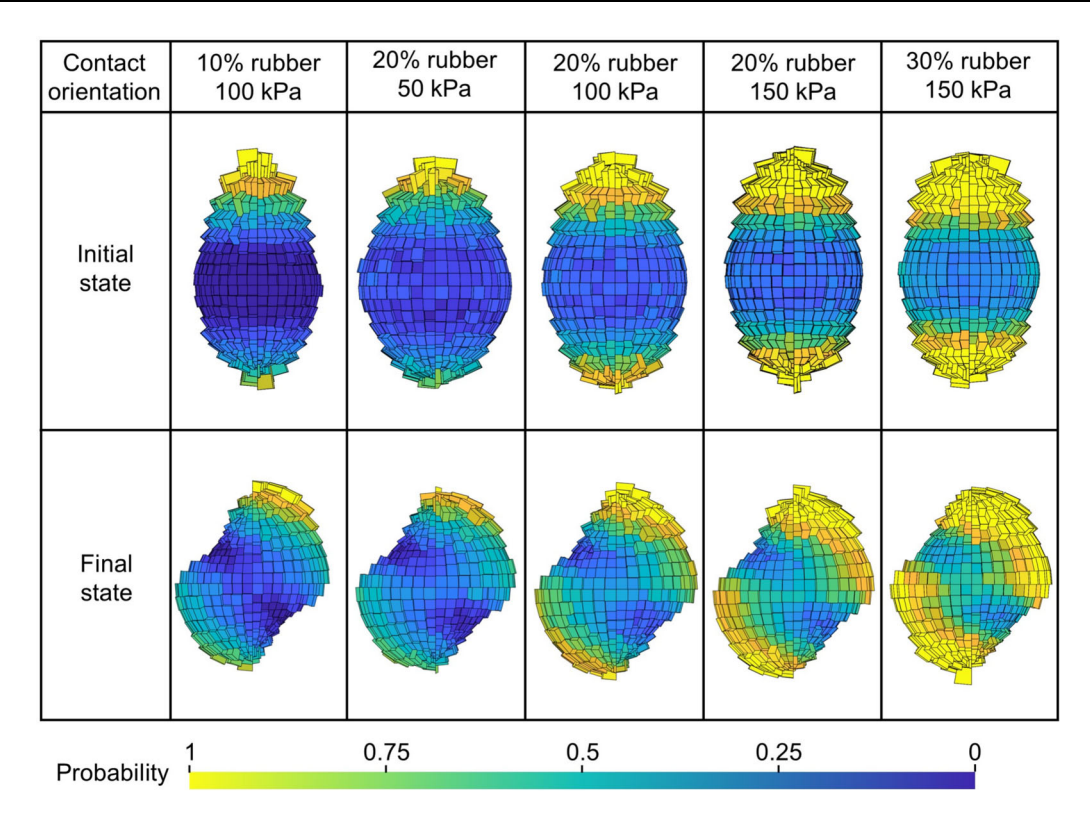


Fig. 19 Distribution of contact normal orientation for inter-particle contacts

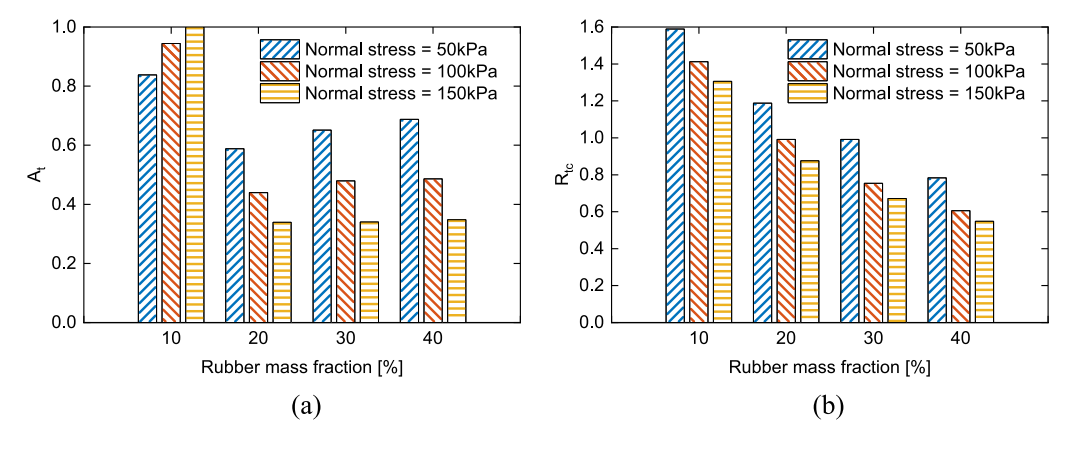


Fig. 20 Effects of normal stress and rubber mass fraction on a the normalized tensile force and b the ratio of the tensile to the compress force of rubber fibers

Figure 24 illustrates evaluation of the average bending angle of all of the rubber fibers within the sand-rubber mixture under different normal stress. During the shearing process, the average bending angle of the rubber fibers decreases linearly, indicating a progressive increase in bending degree of the rubber fibers. Under the same normal stress, the degree of bending deformation in rubber increases with the growth of the mass fraction and stabilizes when the rubber mass fraction reaches 30%. The normal stress also contributes to the bending deformation of rubber fibers, but its impact is weak and can be

considered negligible. It can be further inferred that the increase in rubber mass fraction leads to more entanglement between the rubber particles, which reduces the stable structure formed by the interaction between rubber and sand particles. As a result, the rubber undergoes greater bending deformation.

4.3 Effect of particle shape on shear behavior

Many previous studies have relied on the simplified DEM model to investigate the mechanical behavior of sand-



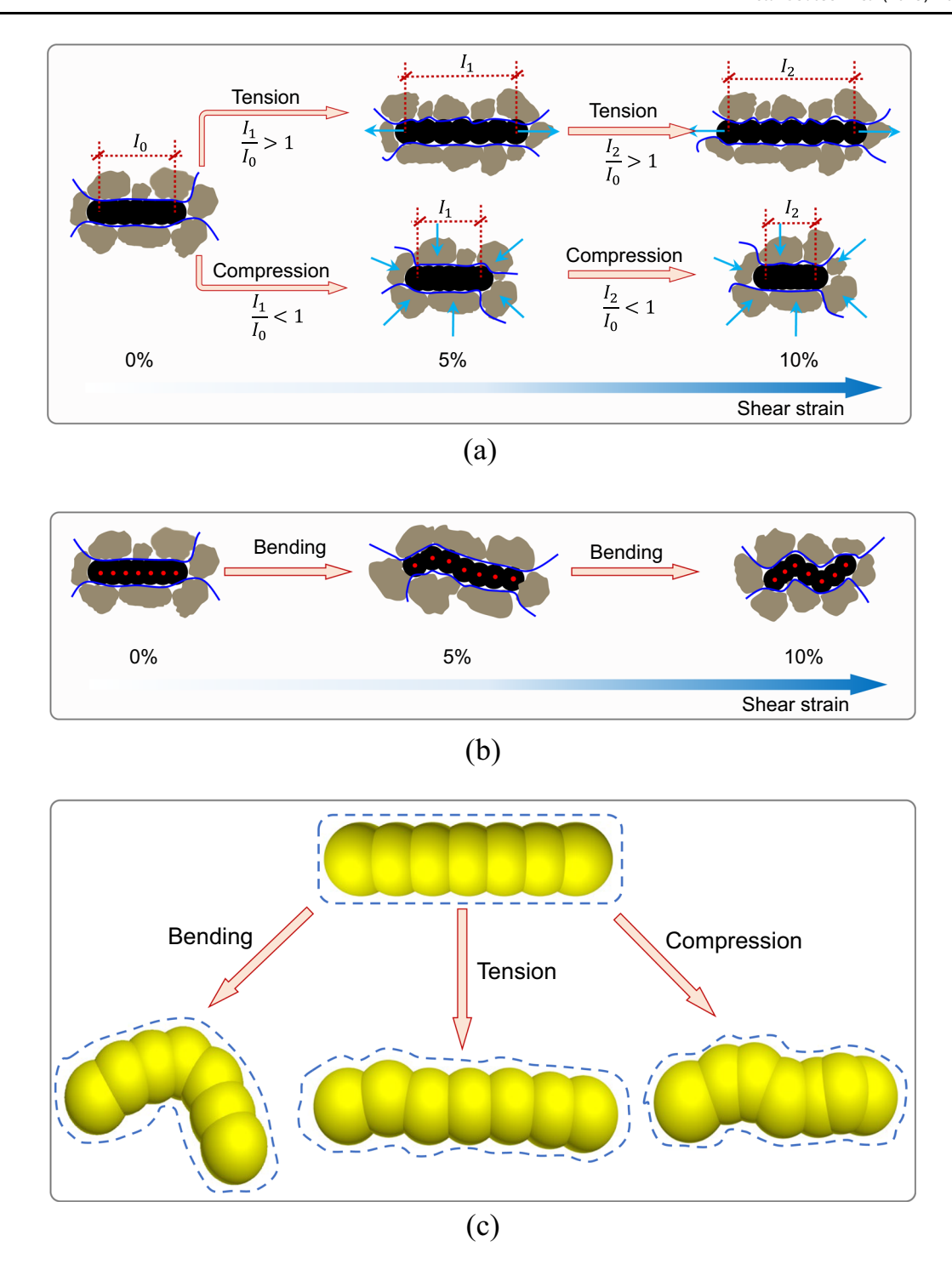


Fig. 21 Two deformation modes of rubber fibers: a axial deformation, b bending and c rubber fiber in simulation

rubber mixtures, in which sand and rubber particles are modeled with spherical particles [28, 68]. This simplification may introduce potential inaccuracies in the simulation results. For instance, the sharp angles on the surfaces of the sand particles cause interlocking between particles, while the rubber fibers fill more of the spaces between the shaped sand particles, resulting in significant particle

rearrangement under shearing. To shed more light on this issue, the effect of the particle shape on the shear behavior is investigated by simulating rubber-sand mixtures with both simplified model and the current model, as shown in Fig. 25. It should be noted that this work focuses specifically on the effect of sand particle shape, while the particle model for rubber fibers remains unchanged. As a



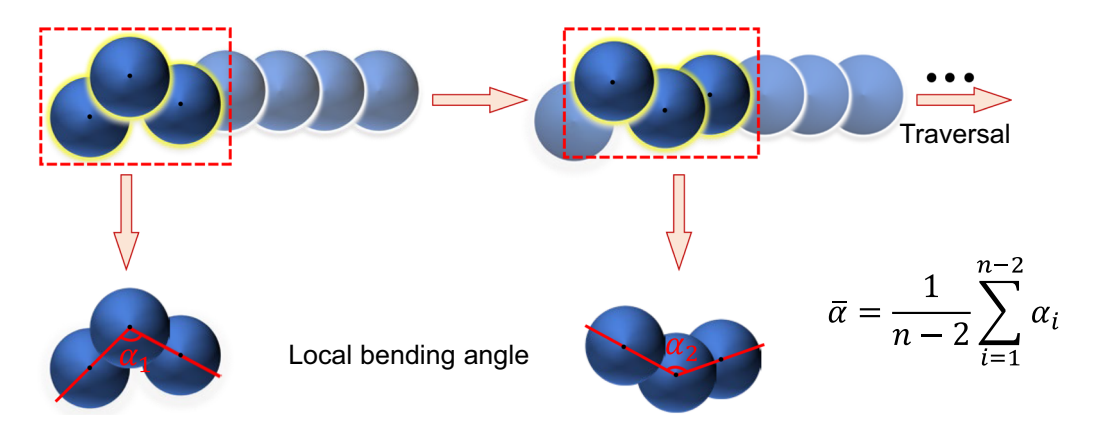


Fig. 22 Definition of the average bending angle

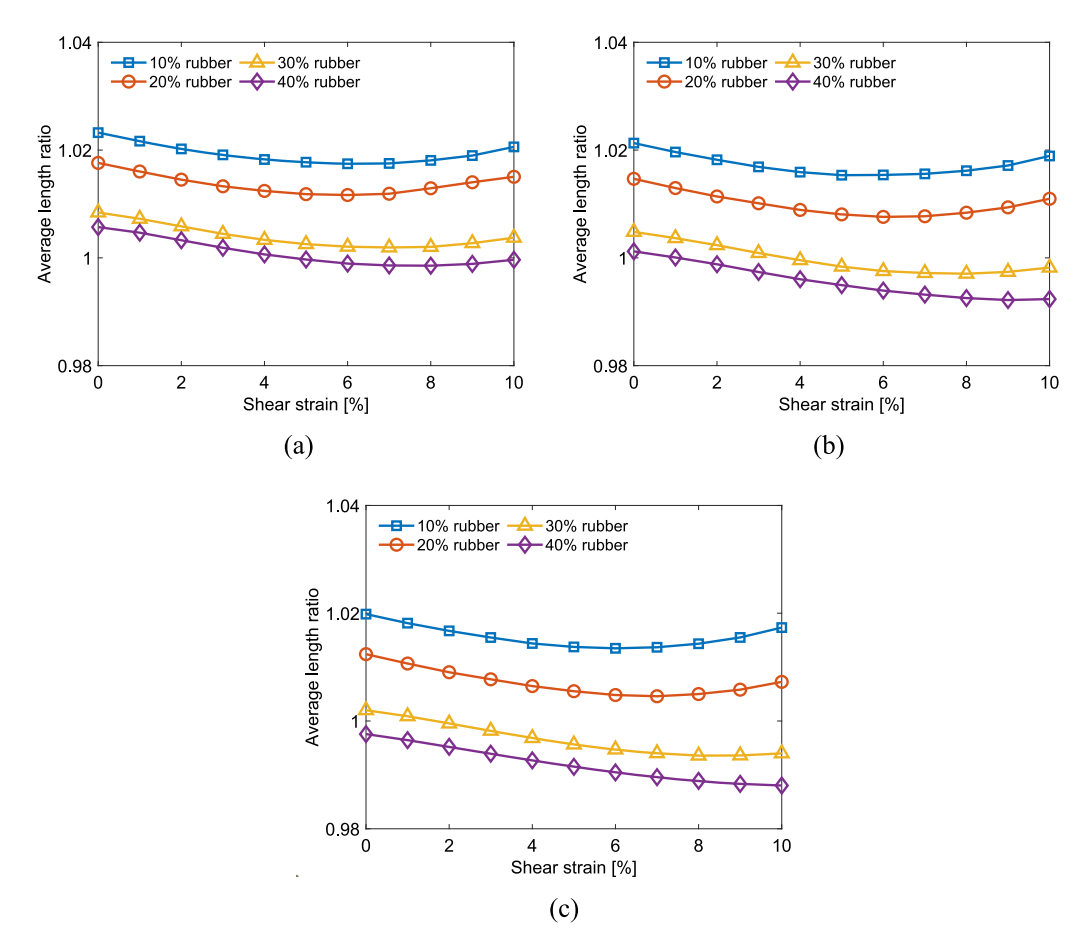


Fig. 23 Evolutions of the average length ratio duiring shearing process: a 50 kPa, b 100 kPa, and c 150 kPa

comparison, two additional cases of DEM simulations are performed. The first case uses the same input parameters for the linear contact model but with simple spherical particles, i.e., no consideration of particle shapes. The second case also uses spherical shaped particles but incorporates rolling resistance in linear contact model (rrlinear), where the rolling resistance coefficient is 0.05 [13]. To eliminate the effect of packing randomness, the

particle configurations of the specimens in the simplified model and the current model are kept consistent.

The macroscopic mechanical behaviors of sand-rubber mixtures modeled with three different models are presented in Fig. 26. Results indicate that both simplified models exhibit strain-softening behavior, whereas the current model demonstrates the continuous hardening behavior, which aligns with observations reported in previous studies [9, 23, 25]. In terms of volumetric strain, the simplified



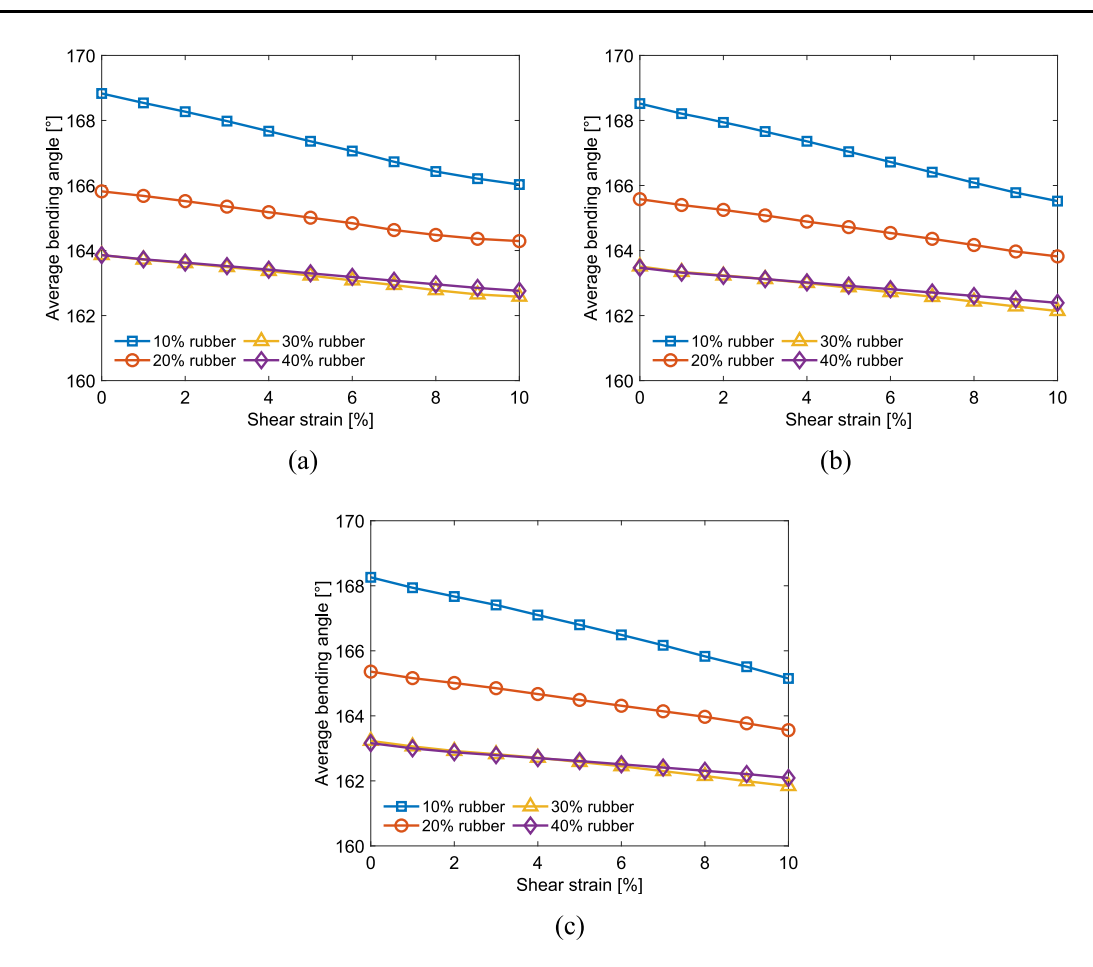


Fig. 24 Evaluation of the average bending angle $\overline{\alpha}$ duiring shearing process: a 50 kPa, b 100 kPa, and c 150 kPa

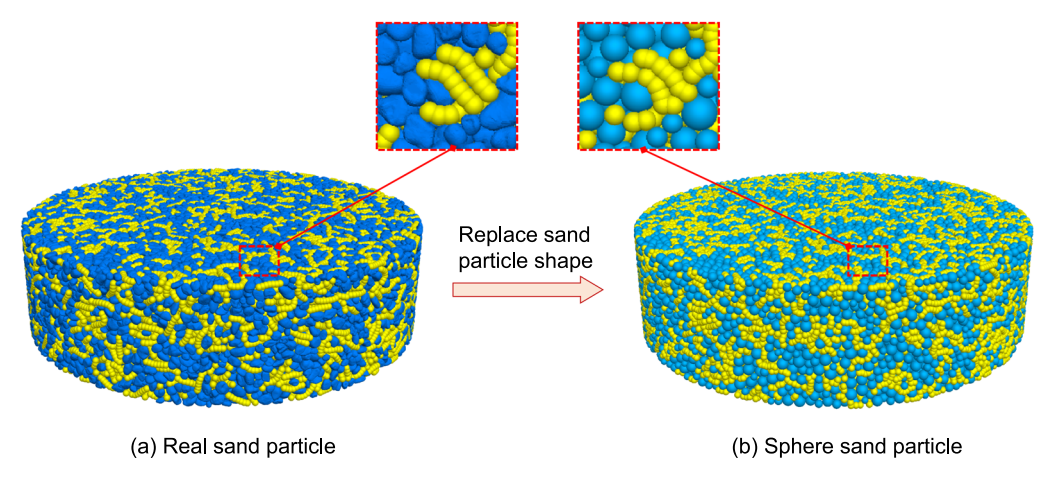


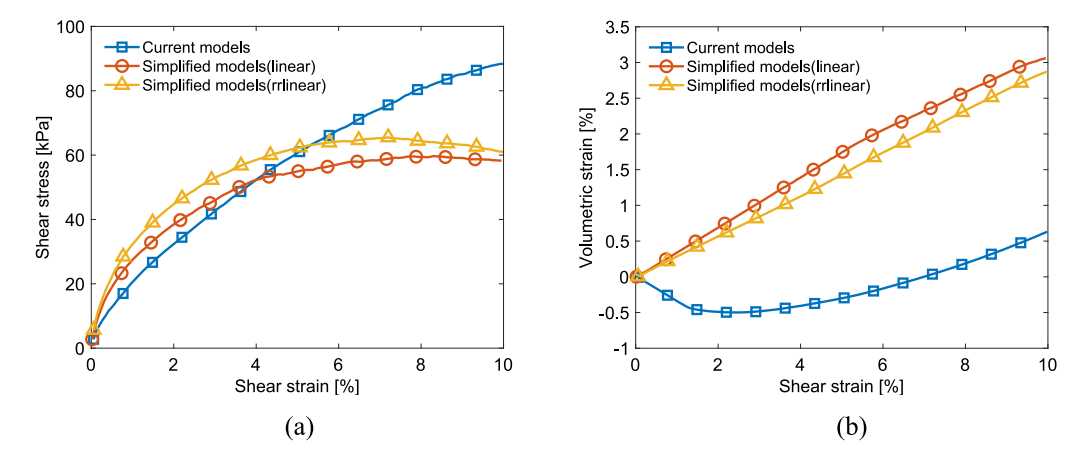
Fig. 25 Particle specimens of a the current model and b the simplified model

model exhibits continuous dilative behavior, whereas the current model shows contractive-to-dilative behavior. This is because the pores between real shape particles are more easily filled, particularly by highly deformable and flexible rubber fibers.

Particle shape also influences the microscopic mechanical behavior. Figure 27 illustrates these differences by

monitoring the contribution of different contact types to the strong contact network after shearing. The results indicate that, compared to simplified model, the sand-sand contacts in the current model make a greater contribution to the strong contact network. Because angular particles have stronger interlocking among particles, the S–S contacts can





25

Fig. 26 The macroscopic mechanical behavior differences of sand particle shapes: a shear stress and b volumetric strain

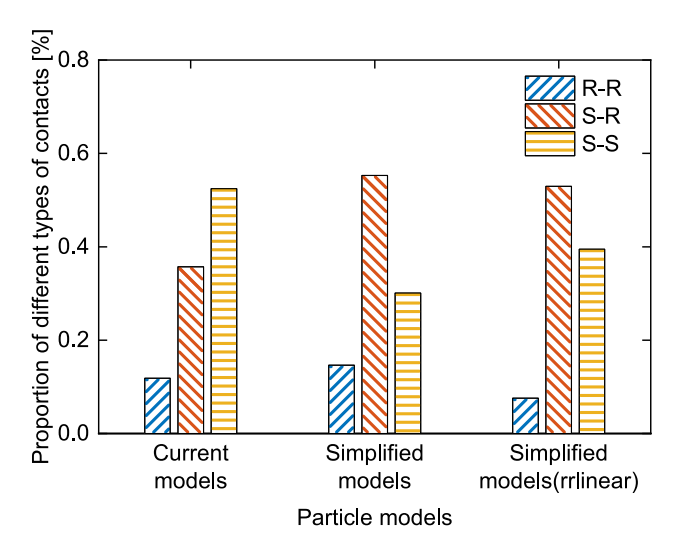


Fig. 27 Contribution of different contact types to strong contact networks in different particle models

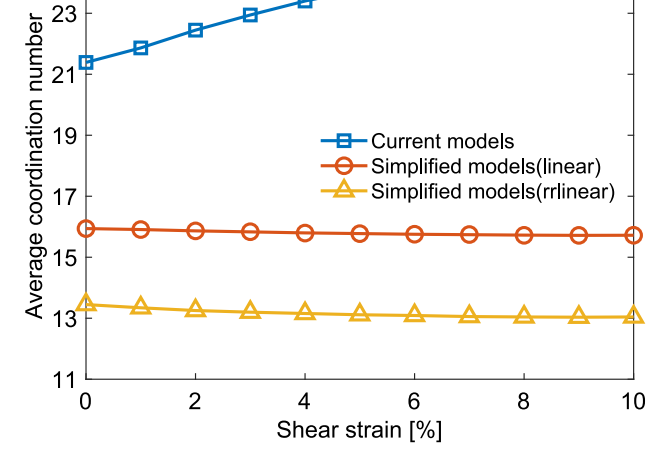


Fig. 28 Evolution of the average coordination number duiring shearing process

bear more external force and contribute to the overall strong contact network.

Particle shape also influences the microscopic mechanical behavior. Figure 27 illustrates these differences by monitoring the contribution of different contact types to the strong contact network after shearing. The results indicate that, compared to simplified model, the sand-sand contacts in the current model make a greater contribution to the strong contact network. Because angular particles have stronger interlocking among particles, the S–S contacts can bear more external force and contribute to the overall strong contact network.

The evolution of the average coordination number during the shearing process is further investigated, with the results presented in Fig. 28. The average coordination number of the current model gradually increases throughout shearing, while that in the simplified model remains almost unchanged with a much lower value, and the

average coordination number of the other simplified model (rrlinear) has an even lower value and also remains almost constant during the shear process. This behavior is attributed to the real sand particles typically have irregular shapes with sharp edges or corners. During the direct shear process, particles undergo rearrangement and rotation, which leads to a continuous increase in the coordination number of real-shaped sand particles. The rearrangement and rotation of particles have little impact on the number of contacts between sphere particles.

Besides, the variation in bending angles of three different DEM models during shearing is also investigated, as shown in Fig. 29. The results indicate that the average bending angle of the simplified models are smaller than that of the current model and decreases rapidly during the shearing process. This is due to the larger internal voids among spherical sand particles, coupled with relatively limited particle rearrangement. The interlocking between



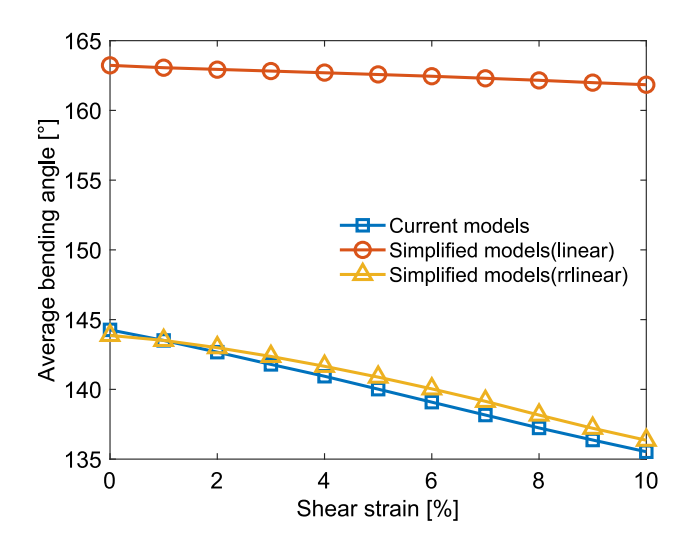


Fig. 29 The average bending angle change of different particle models

sphere particles and rubber is relatively weak, and the rubber is progressively compressed by the sand particles, resulting in stronger bending deformation.

Overall, the study underscores the importance of using sand particles with realistic shapes in simulations of sandrubber mixtures to achieve more accurate mechanical properties at both macro and microscale.

5 Conclusion

This work presents a DEM modeling approach of the sandrubber mixtures in consideration of the realistic shape of particles and the deformability of rubber fibers. The calibrated DEM model can successfully capture the behavior of the sand-rubber mixtures. The irregular-shaped rigid sand particles are simulated with the clump method, while the deformable rubber particles are approximated by bonding spheres into clusters. Subsequently, the DEM parameters of sand-rubber mixtures are calibrated by a series of laboratory tests. Then, by simulating the direct shear test, the mechanical behavior of sand-rubber mixtures is comprehensively investigated from both macroscopic and microscopic perspectives, considering the influence of rubber mass fraction, normal stress, and particle shape. A key focus of our study is the comprehensive examination of the deformation mechanism of rubber-sand mixtures, particularly the deformation and internal force of rubber particles. The main conclusions of this study are summarized as follows:

(1)As the rubber mass fraction increases, the peak shear stress decreases and shifts backward, while dilation is suppressed, particularly under high normal stress. This can be microscopically explained by the lower elastic modulus of rubber-rubber and sand-rubber interactions, which causes samples with higher rubber mass fractions to exhibit greater compressibility, making them more prone to deformation during shearing.

(2)An increase in the mass fraction of rubber reduces the bending angle of rubber fibers, whereas the normal stress contributes to the bending, as demonstrated by the newly proposed descriptor of the average bending angle.

(3)The axial deformation of rubber fibers depends on the rubber mass fraction and normal stress. The rubber fibers predominantly experience tension in samples with low rubber mass fractions and normal stresses. As the rubber mass fraction and normal stress increase, the deformation type of rubber fibers changes from tension to compression.

(4)The shape of particles plays a crucial role in the mechanical behavior of rubber-sand mixtures, both at the macroscopic and microscopic levels. At the macroscale, simplified models that assume spherical particles will underestimate the mixture's shear strength and overestimate its volumetric expansion. At the microscale, simplified models cannot capture the contribution of sand particles to the contact network and fail to consider the pronounced deformation of rubber fibers.

(5)The bending deformation of rubber fibers significantly reduces the overall stiffness of mixtures, leading to a decrease in shear strength and an increased tendency for strain hardening at high rubber content. Additionally, the enhanced S-R contact network alters the force chain transmission path, while the synergistic axial compression of the rubber fibers suppresses volumetric dilation. Overall, these microscopic mechanisms account for the macroscopic mechanical behavior of increased compressibility and reduced softening as rubber content rises.

Acknowledgements This work has been financially supported by the National Key R&D Program of China (2023YFC3009400).

Author's contribution PW contributed to methodology, conceptualization, funding acquisition, and writing-original draft; JG contributed to visualization, methodology, formal analysis, and data curation; SH contributed to visualization and writing-review and editing; BL contributed to writing-review and editing; CX contributed to resources and supervision writing-review and editing.

Funding Open access funding provided by The Hong Kong Polytechnic University.

Data availability Data will be made available on reasonable request.

Declarations

Conflict of interest The authors declare no competing interests.

Open Access This article is licensed under a Creative Commons Attribution 4.0 International License, which permits use, sharing,



adaptation, distribution and reproduction in any medium or format, as long as you give appropriate credit to the original author(s) and the source, provide a link to the Creative Commons licence, and indicate if changes were made. The images or other third party material in this article are included in the article's Creative Commons licence, unless indicated otherwise in a credit line to the material. If material is not included in the article's Creative Commons licence and your intended use is not permitted by statutory regulation or exceeds the permitted use, you will need to obtain permission directly from the copyright holder. To view a copy of this licence, visit http://creativecommons.org/licenses/by/4.0/.

References

- AbdelRazek A, El-Sherbiny RM, Lotfi HA (2018) Mechanical properties and time-dependent behaviour of sand-granulated rubber mixtures. Geomech Geoengin 13:288–300. https://doi.org/ 10.1080/17486025.2018.1440013
- Ahn I-S, Cheng L (2014) Tire derived aggregate for retaining wall backfill under earthquake loading. Constr Build Mater 57:105–116. https://doi.org/10.1016/j.conbuildmat.2014.01.091
- Al-Rkaby AHJ (2019) Strength and deformation of sand-tire rubber mixtures (STRM): an experimental study. Stud Geotech Mech 41:74–80. https://doi.org/10.2478/sgem-2019-0007
- Anbazhagan P, Manohar DR, Rohit D (2017) Influence of size of granulated rubber and tyre chips on the shear strength characteristics of sand-rubber mix. Geomech Geoengin 12:266–278. https://doi.org/10.1080/17486025.2016.1222454
- Ari A, Akbulut S (2022) Effect of particle size and shape on shear strength of sand-rubber granule mixtures. Granul Matter 24:126. https://doi.org/10.1007/s10035-022-01287-7
- Ari A, Akbulut S (2024) Investigation of micro-scale shear response of sand-rubber granule mixture in terms of particle shape and grain scale deformability effects. Particuology 90:452–469. https://doi.org/10.1016/j.partic.2024.01.013
- Asadi M, Thoeni K, Mahboubi A (2018) An experimental and numerical study on the compressive behavior of sand-rubber particle mixtures. Comput Geotech 104:185–195. https://doi.org/ 10.1016/j.compgeo.2018.08.006
- 8. Bao X, Bao Z, Shen J et al (2025) An optimization DEM modelling method for soil-fibre undrained cyclic loading tests model based on the influence range of fibre. Comput Geotech 177:106846. https://doi.org/10.1016/j.compgeo.2024.106846
- Cabalar AF (2011) Direct shear tests on waste tires-sand mixtures. Geotech Geol Eng 29:411–418. https://doi.org/10.1007/ s10706-010-9386-5
- Cai C, Ma W, Zhou Z et al (2019) Laboratory investigation on strengthening behavior of frozen China standard sand. Acta Geotech 14:179–192. https://doi.org/10.1007/s11440-018-0648-3
- Chao Z, Zhou J, Shi D, Zheng J (2025) Particle size effect on the mechanical behaviour of coral sand - geogrid interfaces. Geosynth Int 1–44. https://doi.org/10.1680/jgein.24.00143
- Chen R, Zhao T, Wu Z et al (2023) Experimental investigation on particle breakage behavior of marine silica sand under high-stress triaxial shear. J Mar Sci Eng 11:1825. https://doi.org/10.3390/ jmse11091825
- Chen W-B, Zhou W-H, Dos Santos JA (2020) Analysis of consistent soil–structure interface response in multi–directional shear tests by discrete element modeling. Transp Geotech 24:100379. https://doi.org/10.1016/j.trgeo.2020.100379
- Cheng Z, Wang J (2021) An investigation of the breakage behaviour of a pre-crushed carbonate sand under shear using X-ray micro-tomography. Eng Geol 293:106286. https://doi.org/ 10.1016/j.enggeo.2021.106286

- Cheng Z, Wang J, Xiong W (2024) A machine learning-based strategy for experimentally estimating force chains of granular materials using X-ray micro-tomography. Géotechnique 74:1291–1303. https://doi.org/10.1680/jgeot.21.00281
- Cheng Z, Wang J, Xu D, Fan X (2024) DEM study on the micromechanical behaviour of sand-clay mixtures. Powder Technol 435:119400. https://doi.org/10.1016/j.powtec.2024. 119400
- Cheng Z, Wang J, Zhou B, Xiong W (2023) The micro-mechanical behaviour of sand-rubber mixtures under shear: a numerical study based on X-ray micro-tomography. Comput Geotech 163:105714. https://doi.org/10.1016/j.compgeo.2023. 105714
- Chew K, Chiaro G, Vinod JS et al (2022) Direct shear behavior of gravel-rubber mixtures: discrete element modeling and microscopic investigations. Soils Found 62:101156. https://doi.org/10. 1016/j.sandf.2022.101156
- 19. Chiaro G, Tasalloti A, Chew K, et al (2022) Macro and microscale engineering response of rigid-soft gravel-rubber inclusions: insights from detailed laboratory and DEM numerical investigations. In: Gupta AK, Shukla SK, Azamathulla H (eds) Advances in construction materials and sustainable environment. Springer Singapore, Singapore, pp 11–27
- Contreras-Marín E, Anguita-García M, Alonso-Guzmán EM et al (2021) Use of granulated rubber tyre waste as lightweight backfill material for retaining walls. Appl Sci 11:6159. https://doi.org/10. 3390/app11136159
- Cundall PA, Strack ODL (1979) A discrete numerical model for granular assemblies. Géotechnique 29:47–65. https://doi.org/10. 1680/geot.1979.29.1.47
- D18 Committee Test Method for Direct Shear Test of Soils Under Consolidated Drained Conditions
- Dai B-B, Liu Q, Mao X et al (2023) A reinterpretation of the mechanical behavior of rubber-sand mixtures in direct shear testing. Constr Build Mater 363:129771. https://doi.org/10.1016/ j.conbuildmat.2022.129771
- Ding Y, Zhang J, Chen X et al (2021) Experimental investigation on static and dynamic characteristics of granulated rubber-sand mixtures as a new railway subgrade filler. Constr Build Mater 273:121955. https://doi.org/10.1016/j.conbuildmat.2020.121955
- Enquan Z, Qiong W (2019) Experimental investigation on shear strength and liquefaction potential of rubber-sand mixtures. Adv Civ Eng 2019:5934961. https://doi.org/10.1155/2019/5934961
- Fu R, Yang B, Hu X et al (2023) A micromechanical investigation of sand-rubber mixtures using the discrete element method. Eng Geol 318:107106. https://doi.org/10.1016/j.enggeo.2023. 107106
- Gong L, Nie L, Liu C, Xu Y (2020) Modelling triaxial tests on fibre-reinforced sands with different fibre orientations using the discrete element method. KSCE J Civ Eng 24:2268–2280. https:// doi.org/10.1007/s12205-020-1050-x
- 28. Gong L, Nie L, Xu Y et al (2019) Discrete element modelling of the mechanical behaviour of a sand-rubber mixture containing large rubber particles. Constr Build Mater 205:574–585. https://doi.org/10.1016/j.conbuildmat.2019.01.214
- Guo Y, Markine V, Qiang W et al (2019) Effects of crumb rubber size and percentage on degradation reduction of railway ballast. Constr Build Mater 212:210–224. https://doi.org/10.1016/j.con buildmat.2019.03.315
- Haiyang Z, Fan Y, Chen P, Yingyao C (2024) Seismic performances of the wrapped retaining wall backfilled with polypropylene fiber reinforced rubber-sand mixture. Geotext Geomembr 52:542–553. https://doi.org/10.1016/j.geotexmem. 2024.02.001
- 31. He S-H, Ding Z, Wang M-X, He H (2025) Impact of plane strain state on the long-term cyclic behavior of sand under true triaxial



- tests. Transp Geotech, 101512. https://doi.org/10.1016/j.trgeo. 2025.101512
- He S-H, Yin Z-Y, Ding Z, Li R-D (2024) Particle morphology and principal stress direction dependent strength anisotropy through torsional shear testing. Can Geotech J cgj-2023–0717. https://doi.org/10.1139/cgj-2023-0717
- He S-H, Yin Z-Y, Ibraim E, Ding Z (2025) Face mask chipsreinforced sands under monotonic and cyclic torsional shearing. Géotechnique, pp 1–46. https://doi.org/10.1680/jgeot.24.01180
- Huang S, Huang L, Lai Z, Zhao J (2023) Morphology characterization and discrete element modeling of coral sand with intraparticle voids. Eng Geol 315:107023. https://doi.org/10.1016/j.enggeo.2023.107023
- 35. Huang S, Wang P, Lai Z et al (2024) Machine-learning-enabled discrete element method: the extension to three dimensions and computational issues. Comput Methods Appl Mech Eng 432:117445. https://doi.org/10.1016/j.cma.2024.117445
- Jin Z, Liu J, Ma G et al (2025) How does the largest cluster in the strong network rule granular soil mechanics? A DEM study. Int J Numer Anal Methods Geomech 49:839–859. https://doi.org/10. 1002/nag.3903
- Kowalska M, Chmielewski M (2017) Mechanical parameters of rubber-sand mixtures for numerical analysis of a road embankment. IOP Conf Ser Mater Sci Eng 245:052003. https://doi.org/ 10.1088/1757-899X/245/5/052003
- 38. Lai H-J, Zheng J-J, Zhang J et al (2014) DEM analysis of "soil"-arching within geogrid-reinforced and unreinforced pile-supported embankments. Comput Geotech 61:13–23. https://doi.org/10.1016/j.compgeo.2014.04.007
- 39. Li R, Hu X, Chen F et al (2022) A systematic framework for DEM study of realistic gravel-sand mixture from particle recognition to macro- and micro-mechanical analysis. Transp Geotech 34:100693. https://doi.org/10.1016/j.trgeo.2021.100693
- Li W, Kwok CY, Sandeep CS, Senetakis K (2019) Sand type effect on the behaviour of sand-granulated rubber mixtures: Integrated study from micro- to macro-scales. Powder Technol 342:907–916. https://doi.org/10.1016/j.powtec.2018.10.025
- 41. Li Z, Wang YH, Ma CH, Mok CMB (2017) Experimental characterization and 3D DEM simulation of bond breakages in artificially cemented sands with different bond strengths when subjected to triaxial shearing. Acta Geotech 12:987–1002. https:// doi.org/10.1007/s11440-017-0593-6
- Li R, Yin Z-Y, He S-H (2025) 3D reconstruction of arbitrary granular media utilizing vision foundation model. Appl Soft Comput 169:112599. https://doi.org/10.1016/j.asoc.2024.112599
- Liang W (2024) A mortar segment-to-segment frictional contact approach in material point method. Comput Methods Appl Mech Eng
- 44. Liu L, Cai G, Zhang J et al (2020) Evaluation of engineering properties and environmental effect of recycled waste tiresand/soil in geotechnical engineering: a compressive review. Renew Sustain Energy Rev 126:109831. https://doi.org/10.1016/ i.rser.2020.109831
- Liu Y, Liao X, Li L, Mao H (2020) Discrete element modelling of the mechanical behavior of sand-rubber mixtures under true triaxial tests. Materials 13:5716. https://doi.org/10.3390/ ma13245716
- Liu J, Wu X, Jiang J et al (2023) A network-based investigation on the strong contact system of granular materials under isotropic and deviatoric stress states. Comput Geotech 153:105077. https:// doi.org/10.1016/j.compgeo.2022.105077
- Liu D, Lyu M-Z (2024) Capturing the random mechanical behaviour of granular materials: a comprehensive stochastic discrete-element method study. Géotechnique 1–14. https://doi. org/10.1680/jgeot.23.00467

- 48. Lu Y, Jin W, Klinger J et al (2021) Flow characterization of compressible biomass particles using multiscale experiments and a hypoplastic model. Powder Technol 383:396–409. https://doi. org/10.1016/j.powtec.2021.01.027
- Lu Y, Jin W, Klinger JL, Dai S (2023) Effects of the moisture content on the flow behavior of milled woody biomass. ACS Sustain Chem Eng 11:11482–11489. https://doi.org/10.1021/acs suschemeng.3c01344
- Lv Y, Yang S, He Y et al (2023) Discrete element analysis of sand-tyre chips mixtures with different tyre chip orientations under triaxial compression tests. Constr Build Mater 365:130081. https://doi.org/10.1016/j.conbuildmat.2022.130081
- Madhusudhan BR, Boominathan A, Banerjee S (2019) Factors affecting strength and stiffness of dry sand-rubber tire shred mixtures. Geotech Geol Eng 37:2763–2780. https://doi.org/10. 1007/s10706-018-00792-y
- Moghaddas Tafreshi SN, Joz Darabi N, Tavakoli Mehrjardi G, Dawson A (2019) Experimental and numerical investigation of footing behaviour on multi-layered rubber-reinforced soil. Eur J Environ Civ Eng 23:29–52. https://doi.org/10.1080/19648189. 2016.1262288
- Necochea JE, Sáez E, Hanley KJ (2024) Effect of sand particle shape on micromechanical modeling in direct shear testing. Comput Geotech 169:106222. https://doi.org/10.1016/j.compgeo. 2024.106222
- 54. Nie Z, Qi Q, Wang X, Zhu Y (2022) DEM investigation of strain behaviour and force chain evolution of gravel–sand mixtures subjected to cyclic loading. Particuology 68:13–28. https://doi.org/10.1016/j.partic.2021.10.006
- 55. Nitka M, Grabowski A (2021) Shear band evolution phenomena in direct shear test modelled with DEM. Powder Technol 391:369–384. https://doi.org/10.1016/j.powtec.2021.06.025
- Ren ZL, Cheng YP, Xu X (2020) A DEM method for simulating rubber tyres. Géotechnique Lett 10:73–79. https://doi.org/10. 1680/jgele.19.00064
- Rousé PC (2018) Relation between the critical state friction angle of sands and low vertical stresses in the direct shear test. Soils Found 58:1282–1287. https://doi.org/10.1016/j.sandf.2018.06.
- Shi J, Guo P (2018) Fabric evolution of granular materials along imposed stress paths. Acta Geotech 13:1341–1354. https://doi. org/10.1007/s11440-018-0665-2
- Shi X, He Z, Zhao J, Liu J (2024) Determination of the size of representative volume element for gap-graded granular materials. Powder Technol 437:119578. https://doi.org/10.1016/j.powtec. 2024.119578
- Song S, Wang P, Yin Z, Cheng YP (2024) Micromechanical modeling of hollow cylinder torsional shear test on sand using discrete element method. J Rock Mech Geotech Eng S1674775524001501. https://doi.org/10.1016/j.jrmge.2024.02. 010
- Sun Q, Hou M, Dias D (2024) Numerical study on the use of soft material walls to enhance seismic performance of an existing tunnel. Undergr Space 15:90–112. https://doi.org/10.1016/j. undsp.2023.08.009
- Sun Q, Xue Y, Hou M (2024) Geotechnical seismic isolation system to protect cut-and-cover utility tunnels using tire-derived aggregates. Soil Dyn Earthq Eng 176:108354. https://doi.org/10. 1016/j.soildyn.2023.108354
- Tang Z, Zhang Z, Zhao L, Xiao S (2025) A microscopic DEM investigation on fracture shearing characteristics of infilled grains with different geometrical shapes in rock discontinuities. Rock Mechanics Bulletin 4(2):100174. https://doi.org/10.1016/j.rockmb.2025.100174
- 64. Tasalloti A, Chiaro G, Banasiak L, Palermo A (2021) Experimental investigation of the mechanical behaviour of gravel-



- granulated tyre rubber mixtures. Constr Build Mater 273:121749. https://doi.org/10.1016/j.conbuildmat.2020.121749
- Tavakoli Mehrjardi Gh, Moghaddas Tafreshi SN, Dawson AR (2012) Combined use of geocell reinforcement and rubber–soil mixtures to improve performance of buried pipes. Geotext Geomembr 34:116–130. https://doi.org/10.1016/j.geotexmem.2012. 05.004
- Tian Y, He H, Senetakis K, Yin Z (2024) DEM analysis of the load transfer mechanism of sand-rubber mixtures subjected to constrained compression. Powder Technol 446:120133. https:// doi.org/10.1016/j.powtec.2024.120133
- 67. Utama KA, Harianto T, Muhiddin AB, Arsyad A (2023) The behavior of dredged soil-shredded rubber embankment stabilized with natural minerals as a road foundation layer. Civ Eng J 9:1256–1270. https://doi.org/10.28991/CEJ-2023-09-05-016
- 68. Wang C, Deng A, Taheri A (2018) Three-dimensional discrete element modeling of direct shear test for granular rubber–sand. Comput Geotech 97:204–216. https://doi.org/10.1016/j.compgeo. 2018.01.014
- 69. Wang T, Wang P, Yin Z et al (2024) Hydro-mechanical analysis of particle migration in fractures with CFD-DEM. Eng Geol 335:107557. https://doi.org/10.1016/j.enggeo.2024.107557
- Wang T, Wang P, Yin Z, Zhang F (2022) DEM-DFM modeling of suffusion in calcareous sands considering the effect of doubleporosity. Comput Geotech 151:104965. https://doi.org/10.1016/j. compgeo.2022.104965
- Wang P, Xu C, Yin Z-Y et al (2024) A DEM-based generic modeling framework for hydrate-bearing sediments. Comput Geotech 171:106287. https://doi.org/10.1016/j.compgeo.2024. 106287
- Wang P, Yin Z, Hicher P, Cui Y (2023) Micro-mechanical analysis of one-dimensional compression of clay with DEM. Int J Numer Anal Methods Geomech 47:2706–2724. https://doi.org/ 10.1002/nag.3597
- 73. Yadav JS, Hussain S, Garg A, Tiwari SK (2019) Geotechnical properties of rubber reinforced cemented clayey soil. Transp

- Infrastruct Geotechnol 6:337–354. https://doi.org/10.1007/s40515-019-00088-5
- Yang N, Chen X, Li R et al (2021) Mesoscale numerical investigation of the effects of fiber stiffness on the shear behavior of fiber-reinforced granular soil. Comput Geotech 137:104259. https://doi.org/10.1016/j.compgeo.2021.104259
- Yang SQ, Tian WL, Ranjith PG, Liu XR, Chen M, Cai W (2022)
 Three-dimensional failure behavior and cracking mechanism of rectangular solid sandstone containing a single fissure under triaxial compression. Rock Mechanics Bulletin 1(1):100008. https://doi.org/10.1016/j.rockmb.2022.100008
- Yoon S, Prezzi M, Siddiki NZ, Kim B (2006) Construction of a test embankment using a sand-tire shred mixture as fill material. Waste Manag 26:1033–1044. https://doi.org/10.1016/j.wasman. 2005.10.009
- Zhang J-Q, Wang X, Yin Z-Y (2023) DEM-based study on the mechanical behaviors of sand-rubber mixture in critical state. Constr Build Mater 370:130603. https://doi.org/10.1016/j.con buildmat.2023.130603
- Zhang J, Wang X, Yin Z-Y, Liang Z (2020) DEM modeling of large-scale triaxial test of rock clasts considering realistic particle shapes and flexible membrane boundary. Eng Geol 279:105871. https://doi.org/10.1016/j.enggeo.2020.105871
- Zhao S, Evans TM, Zhou X (2018) Effects of curvature-related DEM contact model on the macro- and micro-mechanical behaviours of granular soils. Géotechnique 68:1085–1098. https://doi. org/10.1680/jgeot.17.P.158
- Zhuo B, Zhu M, Fang Y et al (2021) Numerical and experimental analyses for rubber-sand particle mixtures applied in high-filled cut-and-cover tunnels. Constr Build Mater 306:124874. https:// doi.org/10.1016/j.conbuildmat.2021.124874

Publisher's Note Springer Nature remains neutral with regard to jurisdictional claims in published maps and institutional affiliations.

